Biotechnology and Bioengineering
DOI 10.1002/bit. 21281

Characterization of the Localized Hydrodynamic Shear Forces and Dissolved Oxygen Distribution in Sparged Bioreactors

Athanas Koynov
Department of Chemical and Biochemical Engineering,
Rutgers University,
Piscataway, NJ 08845-8058, USA

Grétar Tryggvason
Department of Mechanical Engineering,
Worcester Polytechnic Institute,
Worcester, MA 01609-2280, USA

Johannes G. Khinast (corresponding author)
Department of Chemical and Biochemical Engineering,
Rutgers University,
Piscataway, NJ 08845-8058, USA
Phone: (732) 445 2970
Fax: (732) 445 2581
E-mail: Khinast@rutgers.edu

Received April 7, 2006; Accepted November 13, 2006

Abstract

Detailed, high-resolution numerical simulations of the bubbly flows, used for oxygen delivery and mixing in mammalian cell suspensions, have been performed. The hydrodynamics, shear and normal forces, mass transfer and mass transport from and around individual bubbles and bubble clusters were resolved for different operating conditions i.e., Weber, Morton and Schmidt numbers. Suspended animal (e.g., mammalian, insect) cells are known to be susceptible to damage potentially leading to cell death, caused by hydrodynamic stresses and oxygen deprivation. Better knowledge of the magnitude of the shear forces and the extent of mixing of the dissolved oxygen in sparged bioreactors can have a significant impact on their future design and optimization. Therefore, the computed liquid-phase velocity fields were used to calculate and compare the local shear in different types of single bubble wakes and in bubble clusters. Oxygen mass transfer and dissolved oxygen transport were resolved to examine oxygen supply to the cells in the different types of flows.

Keywords**:** deformable bubbles, bubble swarms, animal cell culture, mass transfer, cell damage, shear, hypoxia

1 Introduction

In the last fifty years there has been a significant growth in the number of applications of industrial cell cultures. Bacteria and plant cells are common in many processes, such as the production of colors and flavors for the food industry. The fastest growing area, however, is that of animal cell cultures. Mammalian cells are widely used for the synthesis of viral vaccines, peptide hormones, lymphokines and monoclonal antibodies, as well as other protein-based compounds. Due to high demand, these products are usually made by large-scale processes involving liquid suspensions of cells in large reactors (Arathoon and Birch, 1986; Birch et al., 1987; Lubiniecki, 1990; Wu, 1995). Because of the large volumes, nutrient and oxygen transport become a critical issue and efficient mixing is required to ensure the survival of the cell cultures.

A major factor, taken into consideration during bioreactor design - and often limiting the choice of the mixing scheme - is the magnitude of the liquid-phase shear and normal stresses generated during agitation (Born et al., 1992, Al-Rubeai et al., 1995; Chisti, 2001). All cells are susceptible to stress damage (Chisti and Moo-Young, 1986) and in the past it was believed that mammalian cells, due to their lack of protective wall and their size, were more susceptible to stresses. In contrast, recent studies have shown that (at least with additives) most animal cells can tolerate the typical hydrodynamic conditions in industrial bioreactors (Kunas et al., 1990; Oh et al., 1989; Mollet et al., 2004). However, high stresses often lead to a reduced productivity of the cell suspension. Moreover, in the case of cells attached to micro-carriers limitations in the degrees of freedom for deformation lead to an increased sensitivity towards shear damage.

Numerous publications exist, correlating the rotational speed of mechanical impellers to the stresses in stirred tanks and the ensuing damage to suspended cells (Al-Rubeai et al., 1995; Camacho et al., 2000; Jung et al., 2005; Silva-Santisteban and Filho, 2005). In this communication, however, we report the previously unstudied impact of the hydrodynamics in the bulk of a bubble and air-lift reactor. In our simulations we do not observe stress levels sufficiently high to cause the lysis of most cells. This is consistent with many experimental observations reported in the literature (Tramper et al., 1988;

Jobses et al., 1991; Martens et al., 1992), which also show that highly damaging stresses are observed almost exclusively at the free surface due to bubble bursting (Handa et al., 1987; Cherry and Hulle, 1992; Chisti, 1993; Dey et al., 1997, Meier et al., 1999; Dey and Emery, 1999, Chisti, 2001). Nevertheless, even sub-critical stresses can cause cell stress and may lead to cell death after prolonged exposure (Al-Rubeai et al., 1995). Hydrodynamic forces can alter the properties of the cell membrane, leading to increased leakage and passive transport, as well as a breakdown in the electron transport chain, eventually culminating in the death of the cell (Abu-Reesh and Kargi, 1992). Another potential source of cell damage is the hypoxic environment resulting from insufficient oxygen supply to the suspended cells (Zhang et al., 1995; Al-Rubeai and Singh, 1998). Even in processes, in which the cells aren't the final product, post-apoptotic cell lysis can decrease the efficiency of the reactor, by contaminating the liquid phase with cytosolic material, and thus, increasing downstream product purification costs (Chisti et al., 2001).

Cell stress and culture productivity are a function of a cell's or a cell cluster's microenvironment. Thus, the focus of this paper is a *localized* description of the hydrodynamic flow-fields and dissolved oxygen availability observed in swarms of deformable bubbles. In this work we use first-principles methods, i.e., a direct numerical simulation of the multiphase flow and the oxygen transport, augmented by a model for cell advection by the flow. This model has the ability to track large numbers of individual cells, as they are transported in the reactor volume over extended periods of time. The stresses experienced by each cell at each point in time can thus be determined to obtain a picture of the actual magnitude of the cells' exposure to shear and extensional stress. To the best of our knowledge, we are the first group to report such a detailed study.

It is important to emphasize, that the aim of this work is the detailed analysis of stress and oxygen transport *on a micro-scale*. We do not intend to simulate an entire bioreactor. Instead, we provide a tool for the description of the localized phenomena, which may be used to gain a deeper understanding of the conditions cells encounter in industrial suspensions. Since all effects in bioreactors are highly localized, these micro-simulations provide important insight for the design of gassed bioreactors.

2 Background

Ease of design and operation, low power requirements, uniform mixing characteristics throughout the entire volume, and relatively high oxygen mass-transfer rates make *sparged reactors* a good choice for the culture of animal cells. However, due to the complexity of the multiphase flow, calculation of the liquid-phase velocity profiles and stress field inside a sparged reactor is a formidably difficult task. This complexity is due to numerous factors, such as the dynamically changing bubble shape, size and rise velocity, bubble-bubble interactions, coalescence, break-up and clustering effects among many others. Even though the stress fields typical of bubbly flows are lower than the ones observed around impeller blades, the motion of bubbles still has the potential to cause damage or stress to suspended cells. Tramper et al. (1987) studied typical airlift reactors and deduced that shear rates, sufficient to cause cell lysis, can be observed only at the free surface of the reactor, where the bursting of bubbles created harsh hydrodynamic conditions. Subsequent studies of cell damage caused by bubble bursting were performed by Hand-Corrigan et al. (1989), Kunas and Papoutsakis (1990), Chalmers and Bavarian (1991), Wu (1995) and Camacho et al. (2000) among others.

While the hydrodynamic forces in the sparger and riser zones of a typical bioreactor are insufficient to destroy most cells, prolonged exposure to sub-lethal stress levels can also lead to cell death. Ziegelstein et al. (1992), after performing experiments with rat aortic endothelial cells on internal walls of glass capillaries, concluded that laminar shear stress can affect the cytosolic pH because of membrane ion leakage even at very low stresses ($\sim 0.05 Nm^{-2}$) and over very short durations (~2 min.). Cone and plate viscometer experiments, carried out by Born et al. (1992) and Al-Rubeai et al. (1993), showed that shear exposure can lead to substantial loss of cell count and viability within 20 minutes.

Most data in the literature correlating hydrodynamics to cell damage are empirical in nature and strongly depend on the specific system. A major step towards building a rational understanding of the subject was made by the group of Chalmers (Garcia-Briones and Chalmers, 1994; Georgiades et al., 2000). In addition, they pointed out the need to distinguish between two types of flows, which differ in their potential to damage the

cells. In shear flows (such as the ones observed between two parallel plates) the rotation of the axes of the principal rates of strain with respect to the liquid will cause the points within the cell subjected to the highest elongation to change with time. In extensional flows (only normal stress components), on the other hands, these will remain constant. A demonstration of their implications has been given by Taylor (Taylor, 1934): a droplet suspended in a liquid and exposed to the same amount of stress breaks in an extensional flow, and fails to do so in a shear flow.

Several different approaches have been considered to minimize the stress-induced damage of animal cells in bubbly flows. One consists of altering the properties of the cell membrane and the nature of the cell-bubble interactions through additives to the cell medium. For example, Pluronic F68 – a frequently used, non-ionic surfactant - has been shown to suppress animal cell damage by decreasing the fluidity of the cell membrane, thus making it less fragile, and by preventing the adhesion of cells to bubbles (Ramirez and Mutharasan, 1992 and Zhang et al., 1995). Recent publications have shown that PF68 can decrease the susceptibility to shear of plant cells as well (Sowana et al., 2002). Other popular additives include bioactive supplements (serum, cholesterol), viscosity enhancing polymers (methylcellulose, CMC and dextran) and surface-active polymers (polyethylene glycol, polyvinyl alcohol) among others.

A second approach, which has been shown to yield positive results for some cell lines, involves controlling the death mechanism itself. Cells exposed to very high levels of shear suffer necrosis, during which the cell membrane ruptures and the contents of the cell spill into the bulk liquid (Al-Rubeai et al., 1995). Exposure to sub-lethal levels of shear, on the other hand can result in cell apoptosis (programmed cell death), defined by a controlled decrease of cell volume, blebbing of the cytoplasm and, ultimately, disintegration of the cell into membrane enclosed apoptotic bodies. By suppressing different stages in the execution of the apoptosis program, cell death can be averted. Examples include the over-expression of Bcl-2 (or any other member of a family of apoptosis suppressing proteins), which can inhibit the release of pro-apoptotic molecules from the cell mitochondria and does prevent cell death (Udaykumar et al., 2001). Bcl-2

over-expression has been shown to offer effective protection from both shear induced (Perani et al., 1998) and hypoxia-induced apoptosis (Simpson et al., 1997). The addition to the medium of caspase-specific peptidic inhibitors that bind to the catalytic site of these proteases, which are critically involved in the apoptotic process in mammalian cells and have an important role in the commitment, amplification and demolition phases of the death program, can also result in the suppressing the apoptosis (Tintó et al., 2002).

Nevertheless, a detailed knowledge of the velocity fields in the suspension phase and - by extension - the stress fields to which the cells are exposed can be invaluable. It can be used to predict the potential for damage of different cell lines with different sensitivities to stress and facilitate the choice of preventive measures against stress damage. An additional benefit of resolving the multiphase hydrodynamics is the ability to anticipate the mass-transfer and mass-transport rates, which control the supply of oxygen to the suspended cells.

Experimental investigations of the flows around individual bubbles are usually based on variations of image analysis and Particle Image Velocimetry (PIV) techniques. A typical example is the work of Tokuhiro *et al.* (1998) that examines the turbulent flows past bubbles using a combination of PIV and an Infrared Shadow Technique to resolve both the liquid-phase velocity field and the bubble contour. Raymond and Rosant (2000) used imaging methods to investigate the dependence of the aspect ratio of non-spherical bubbles on the physical properties of the multi-phase system. Choi *et al.* (2002) implemented a combination of flow visualization techniques and PIV to provide an in-depth look at the motion of deformable gas bubbles in a stagnant liquid. Recently, Bork and coworkers (Bork et al., 2003), successfully applied image analysis and fluorescence methods to study the flow dynamics and mass transfer from single bubbles. Nevertheless, optical methods suffer from the limitations imposed by the medium, i.e., they cannot be applied in opaque media such as cell cultures. Thus, numerical simulations offer a distinct alternative, and several different techniques have been developed and applied, with varying degrees of success. The main challenge in simulating reactive bubbly flows is the proper *resolution and tracking of the gas-liquid interfac*e and the *mass transfer*

through the interface. Methods belonging to the "Marker And Cell" (MAC) and "Volume Of Fluid" (VOF) families perform this task by identifying the two phases directly on a uniform computational grid by using marker variable. Despite the difficulties associated with the accurate description of the interface - somewhat alleviated by the use of level-set methods (Fedkew and Osher, 2001) - these methods are widely used (Brackbill et al., 1992; Scardovelli and Zaleski, 1999; Laekhal et al., 2002; van Wachem and Schouten, 2002). Lagrangian methods (Shopov et al, 1990), in which the grid follows the fluid, have provided useful insight into the mechanisms of the deformation of bubbles. In front tracking methods, a separate, deformable grid is used to track the interface, while the flow is computed on a fixed uniform grid (Glimm et al., 2001; Tryggvason et al., 2001 and Sankaranarayanan et al., 2003). In this work, a method based on the work by Tryggvason is used to study the hydrodynamics of bubbly flows. This method is the first numerical approach ever reported to be able to successfully simulate the complex hydrodynamics, mass transfer, liquid-phase transport and (bio-) chemical reactions around multiple dynamically deforming bubbles.

The influence of the hydrodynamics on the gas-liquid mass transfer has also been subject of considerable scientific interest. Aris (1997) studied the gas-liquid mass transfer during the steady ascending motion of small spherical bubbles. Legendre and Magnaudet (1999) investigated the mass and heat transfer from a spherical bubble in accelerated flows. These studies were recently extended by us (Khinast, 2001; Koynov and Khinast, 2004). Recently, Bothe et al. (2003) performed VOF-based numerical simulations of the mass transfer of a gas from deformable bubbles and bubble chains, and Koynov et al. (2005) successfully used a front-tracking approach to examine the mass transfer from multiple deformable bubbles rising in a cluster.

3 Model and Numerical Methods

For the purposes of this study, a numerical model was developed to provide detailed, high-resolution simulations of the motion of cells suspended in a liquid phase, through which bubbles are sparged. A hybrid front-tracking/front-capturing method (Tryggvason et al., 2001), coupled with chemical species conservation equations was used to simulate the hydrodynamics of bubbly flows, as well as the interfacial mass transfer of oxygen, its

transport in the continuous phase and its subsequent consumption by the suspended cells. Bubble swarms were simulated for different values of the physical parameters, which were cast in dimensionless numbers, i.e., the Morton number $Mo = g\mu_l^4 / (\rho_l \cdot \sigma^3)$ and the Eötvos number $Eo = g\rho_l d_b^2 / \sigma$. From the computational results, the bubble Reynolds number $\mathrm{Re}_b = d_b U_t \rho_l / \mu_l$ and the Weber number $We = d_b U^2{}_t \rho_l / \sigma$ $(= \mathrm{Re}_b^2 \sqrt{Mo / Eo})$ were estimated. For different values of these numbers, bubbles can have various shapes, as well as exhibit different types of wake flows.

In our method, the Navier-Stokes equation describing the fluid flow is integrated on a regular, fixed, two-dimensional grid. It is a single fluid method, which means that a single set of conservation equations is solved for both phases. An immersed boundary type formulation is used to provide the smoothing of the delta functions describing the jump in variable gradients at the bubble interface onto the computational grid. The actual interface is tracked using a separate, one-dimensional moving deformable grid (for more information, see Koynov et al., 2005). The model equations, describing the system, can be written as:

$$\frac{\partial \rho \mathbf{u}}{\partial t} + \nabla \cdot \rho \mathbf{u}\mathbf{u} = -\nabla P + \rho \mathbf{f} + \nabla \cdot \mu\left(\nabla \mathbf{u} + \nabla^T \mathbf{u}\right) + \oint \sigma \kappa' \mathbf{n}' \delta^2 \left(\mathbf{x} - \mathbf{x}'\right) ds' \qquad (1)$$

and

$$\frac{\partial c_{O2}}{\partial t} = -\mathbf{u} \cdot \nabla c_{O2} + D_{O2} \Delta c_{O2} - r_b \,. \qquad (2)$$

The equations are satisfied for the entire computational domain, regardless of discontinuities in material properties. In Eq. (1), **f** is a body force, σ is the surface tension, κ is the curvature of the interface, and δ^2 is a two-dimensional delta-function, equal to the product of δ(x-x') and δ(y-y'). In the species-balance equation (Eq. 2) for dissolved oxygen $c_{O2,}$

$$c_{O2}(x, y, t) = c_{l,O2} H(x, y, t) + c_{g,O2} \left(1 - H(x, y, t)\right), \qquad (3)$$

where $c_{l,O2}$ is the concentration of species oxygen in the liquid phase, and $c_{g,O2}$ is its concentration in the gas phase. The concentration of oxygen in the bubble, i.e, $c_{g,O2}$, is uniformly constant and is equal to the oxygen saturation concentration for the liquid phase. This is a reasonable assumption for the cases, where the characteristic residence time of the bubble is short compared to the mass-transfer time scale. The consumption rate, r_b is the rate, at which the oxygen is consumed in a grid cell and is dependent on the number of (biological) cells in the grid cell. In Eq. (3), H is a Heaviside step function, describing the discontinuities in variable values, which occur at the bubble surface.

The computational domain used in our simulations has a rectangular shape and dimensions of $12 \cdot d_b \times 36 \cdot d_b$, d_b being the average bubble diameter. The hydrodynamic computations were carried out on a 200×600 grid, whereas the mass transport calculation grid had 600×1800 grid cells, due to the need to accurately resolve concentration fields. The fluid velocities were interpolated onto the fine grid using a high-order, continuity-preserving scheme (Koynov et al., 2005). Periodic boundary conditions were implemented at the top, bottom and both walls of the domain, ensuring that a fluid particle exiting the domain from one side will reenter from the other with the same velocity. The same boundary conditions were used for the species transport computations and biological cell advection as well. In Table I, the parameters for our simulations are given, which are typical for many industrial bioreactors. The characteristic length, on which the dimensionless numbers are based, is the equivalent spherical diameter of the bubble, and the characteristic velocity – the terminal rise velocity of the bubble.

The animal cells are assumed to be neutrally buoyant and are modeled as discrete points dispersed through the computational domain. The initial cell spatial distribution is uniform with a cell density of $2.5 \cdot 10^5$cell/ml. The cell motion is modeled as simple Lagrangian advection. Terms describing additional forces acting on the cells (such as drag, lift, added mass, Magnus and Faxen contributions) have been neglected, due to the small cell sizes. For the purposes of cell advection, local velocities are interpolated from their coarse grid values using

$$\mathbf{u}_c = \sum_{i,j} w_{i,j} \mathbf{u}_{i,j} \,, \tag{4}$$

where $\mathbf{u}_c$ is the velocity at the location of the cell, $\mathbf{u}_{i,j}$ are the velocities at the surrounding cell nodes and $w_{i,j}$ are weighing functions. The shear stress acting on each cell is

$$\tau = \mu \left(\frac{\partial u_c}{\partial y} + \frac{\partial v_c}{\partial x} \right), \tag{5}$$

where μ is the liquid viscosity and u_c and v_c are the two components of the liquid velocity at the location of the cell. Extensional components of the flow are $\sigma_x = \mu \partial u_c / \partial x$ and $\sigma_y = \mu \partial v_c / \partial y$, where $\sigma_x = -\sigma_y$ at each point in the flow. In our simulations, more than 500,000 individual cells were tracked.

In order to asses the exposure of the cells to shear over time (=cell stress) in the different hydrodynamic environments simulated, a quantity was introduced labeled for convenience "cell stress level" χ. This quantity is representative of the cumulative influence of the *shear and hypoxia stresses* a cell is exposed to during its residence in the reactor. Normal stresses in the bubble flow are usually lower than the encountered shear stresses. Thus, they have been neglected in the cell stress model. This will be discussed in more detail below.

Rather than using a simple summation of all stresses acting at the location of the cell at each computational time point, a generic stress-level model was developed, based on empirical data from the literature (Abu-Reesh and Kargi 1989). In their study, Abu-Reesh and Kargi subjected hybridoma cells to defined shear stresses in a Searle viscometer for prolonged periods of times and recorded the percentage of dead cells as a function of stress level and exposure duration. The model used here is a mathematical tool, which can be used to demonstrate the difference between the impact that the shear forces in the several flow situations can have on suspended cells. The three coefficients (a_c, b_c and c_c) in our stress model

$$\frac{d\chi}{d\tilde{t}} = \left(a_c \tau^2 + b_c \tau + c_c\right) + H_c, \tag{6}$$

were chosen such, that for a given initial random Gaussian distribution of cell membrane strength, the percentage of dead cells after a given period of exposure to a defined shear stress will match the one suggested by Abu-Reesh and Kargi's results. In equation 6 $\tilde{t}$ is dimensionless time, χ is the cell stress level (it takes values between zero and one, with one corresponding to cell death) and H_c is the hypoxic contribution to cell stress. Since the response of cells to hypoxia is even more varied than their response to shear, the hypoxia-induced damage model strives to serve as a method for the identification of trends than as an accurate prediction tool. For these reasons, a linear dependence on local oxygen availability was chosen:

$$H_c = \begin{cases} 0, & if\ c_{O2} > c_{hp} \\ d_c \dfrac{c_{O2} - c_{hp}}{c_{hp}}, & otherwise \end{cases}, \tag{7}$$

where d_c is a coefficient tailored to yield stress rates consistent with realistic cell behavior. The values of the coefficients used for the stress-level model are given in Table II. Even though it is unlikely to occur at the shear stress levels encountered in our simulations, for the reason of completeness (and because in the future we will extend this work to free surfaces) we considered necrotic cell death via membrane rupture. A model describing this mechanism has been derived by Born et al., (1992). If a cell is assumed to behave like a viscous drop, its deformation, caused by laminar shear will equal:

$$D = \xi \tau \frac{r_c}{\sigma_c}, \tag{8}$$

where τ is the shear stress (as given by Eq. 5), r_c is the cell radius, σ_c is the cell membrane tension and ξ is given by Taylor (1934) as

$$\xi = \frac{19\frac{\mu_i}{\mu} + 16}{16\frac{\mu_i}{\mu} + 16}, \tag{9}$$

where μ_i is the viscosity inside the cell. From Eq. 8, it follows that, for a given deformation D, the membrane tension of a cell will be

$$\sigma_c = \frac{\xi \tau r_c}{D}. \tag{10}$$

If the cell tension σ exceeds a given bursting value, σ_b i.e.

$$\frac{\xi \tau r_c}{D_b} \geq \sigma_b \tag{11}$$

the cell will be destroyed. To account for biological biovariability, the bursting tensions and radii of the cells obey a Gaussian distribution (with a mean bursting tension of $1 \cdot 10^{-3}$ Nm^{-1}, mean cell radius of $1 \cdot 10^{-7}$m. and a standard deviation of 5% for both distributions). A mean value, obtained from literature is used for D_b, in order to simplify computations (Born et al., 1992; Zhang et al., 1992), (see Table II).

4 Results and Discussion

4.1 Hydrodynamics

Depending on the system parameters, the dynamics of the buoyancy driven bubble motion can change dramatically. Figure 1 shows four snapshots of the stream-traces associated with the liquid-phase velocity fields around gas bubbles rising under different conditions. At low Reynolds numbers (Fig. 1a), bubbles rise in straight lines, while retaining an ellipsoidal shape. The bubble wake in this case is steady and has been shown to develop two symmetric recirculation cells at intermediate Reynolds numbers. As the Reynolds number increases, the size of these recirculation cells will increase as well, until a certain critical Reynolds number is reached, when symmetry breaking initiates periodic vortex-shedding in the wake (Fig. 1b). This phenomenon is

characterized by vortices forming periodically on each side of the bubble centerline. After the vortices detach, they are advected downstream, forming a *von Karman* vortex street. It is well known that differences in wake flow dynamics translate into qualitatively different transport and mixing characteristics and can, therefore have a significant impact on the performance of reactive systems in the liquid phase (Koynov and Khinast, 2004).

While the flows in the wakes of single rising bubbles are relatively well studied, less is known about the complex velocity fields developing around multiple bubbles rising simultaneously. Figure (1c and d) shows the stream traces associated with two such velocity fields for two different, nine-bubble clusters. It can be seen that bubble-bubble wake interactions cause even the low-Reynolds-number bubbles to deviate from their linear paths and rise in irregular meandering trajectories. Both snapshots imply complex flows with multiple vortical structures and it can be seen that while the low-Reynolds-number flow is still predominantly vertical, the higher-Reynolds-number case exhibits a significant lateral component. Additionally, closer observations reveal that, in the low-Reynolds-number case, the recirculation zones in the bubble wakes still persist, albeit deformed. These differences in liquid-phase dynamics can be explained by the tendency of the individual bubbles in the two swarms to follow straight and serpentine trajectories, respectively, and the overall cluster behavior can be treated as a combination of single bubble motion and bubble-bubble interactions. This means that the differences in transport characteristics exhibited by the different "single bubble" wakes will, to a certain extent, influence the transport in swarms of multiple bubbles as well. In simpler terms, even though the bubbles in both the low and high Reynolds number cases move in complex non-linear trajectories, the preserved single-bubble wake structure makes the transport characteristics in the low Reynolds number case inferior.

4.2 Cell Stress due to Shear and Normal Stresses

The flow around bubbles rising in different conditions exhibits different local shear and normal stresses and has the potential to impact suspended animal cells at different rates. Figure 2a shows several snapshots of the shear stress fields around rising bubbles for different cases. It can be seen that in the steady wake case, high shear rates are observed,

predominantly in the two recirculation zones (snapshot i) behind the bubble. It is worth noting that the interactions between the bubble and the wake of a preceding bubble are insufficient to change the situation at later times (snapshot iii). In the vortex-shedding wake (snapshot ii), high shear rates are encountered in the wake vortices. The highest rates are associated with the process of growth and shedding. The action of bubble-wake interactions leads to the formation of multiple disconnected high-shear zones associated with the vortical structures or eddies (snapshot iv). These high shear zones are spread over the entire domain, in contrast to the steady wake case, where shear is confined to the back of the bubble. Figure 2b shows the distribution of shear and normal forces in the bubble flow for 9 bubbles rising at two different Reynolds numbers, corresponding to the cases shown in Figure 1c+d. It can be seen that the normal stresses in these bubble flows are significantly lower than the corresponding shear stresses. For example, in the case of Re=75, 90% of all cells have normal stresses lower then 0.5 (normalized value) but shear stresses are as high as 0.9. For this reason, shear stresses were the only stress component considered in the cell stress model. It should be kept in mind however, that in reality, normal stresses may be even more damaging to suspended cells (especially in the case of cells attached to microcarriers). While the simple shear flows in the steady wake case do result in cell elongation, the lines of points within the cell exposed to the highest stretching rates at each time will rotate. This rotation will take these lines of cells from the maximum stretching position to a neutral position and then to a position where the line contracts. This transfer of stress between different axes within the cell leads to a decrease in the damage the cell will suffer. By contrast, in the extensional flows observed along the unstable manifolds of the chaotic saddles typical of unsteady wakes, the line of points within the cell along the direction of maximum elongation will remain the same for all points in time. Thus, no stress relaxation will occur and the damage sustained by the cell will be higher. The notion that, at the same stress, extensional flows will inflict more damage to suspended cells than shear has been introduced and developed (Garcia-Briones and Chalmers, 1994; Georgiades et al., 2000). However, no quantitative data have been published so far.

Figure 3 shows several snapshots at different moments in time of the cumulative shear-related stress level for cells around single bubbles rising in the steady and vortical wake regimes. The ranges of the dimensionless numbers, in terms of which the results are reported, correspond to typical parameter values for realistic bubbly flows. For example, bubbles of size between 2 and 5mm, rising in a liquid of density between 1000 and 1200kg/m^3 and with viscosity between 5 and 50cP will rise with terminal velocities between 0.2 and 0.3m/s, leading to Reynolds number varying between 5 and 150.

It can be seen that in the low and intermediate Reynolds number cases (Fig. 3a, b and c), potential cell damage is confined to the wake region. In the vortex-shedding regime, on the other hand, the zone expands to cover the entire width of the vortex street (Fig. 3 d). Cells in such wakes can be passed from vortex to vortex (Jung et al., 1993; Koynov and Khinast, 2004), thus, remaining trapped in the high shear area for prolonged periods of time and being carried with the bubbles to the surface by this mechanism. Consequently, vortex-shedding bubbles in swarms – in contrast to the ones with closed wakes - will result in a significant net up-flow of cells to the surface of the tank. The two snapshots in Figure 3e and f show a bubble, which, due to the periodic boundary conditions, has reentered its own wake from the bottom of the domain (this situation is representative of the very common occurrence of bubbles being affected by the wakes of a leading bubble). The interactions between the bubble and the von Karman vortices lead to a more pronounced "waviness" of the bubble motion and an expansion of the wake. For the cells, these interactions translate into higher shear over a wider area.

The differences in shear-induced stress in different wakes are quantified in Figure 4, which shows the average, cumulative cell stress level due to exposure to shear as a function of time for the three wakes (low, intermediate and higher Reynolds number). The cumulative stress experienced by each cell has been computed by integrating Eq. 6. The computation of the motion of the cells and the multiphase hydrodynamics are coupled, which allows for shear stresses to be obtained at the location of each cell at each point in time. These stresses are then used to calculate the potential damage incurred by

each cell. The values plotted in Figure 4 are obtained by averaging the cumulative incurred potential damage over all simulated biological cells.

The higher stress level sustained by cells in the intermediate Reynolds number case (as compared to the low Reynolds number one) can be explained by the increased relative gas-liquid velocity, leading to higher shear. Additionally, the appearance of a hyperbolic point in the liquid-phase velocity field, due to the formation of recirculation zones, causes fluid element stretching and compression (along the hyperbolic point's unstable and stable manifolds respectively), which can be detrimental for the suspended cells (for more information on critical points in bubble wakes see Koynov and Khinast, 2004). The increase in shear exposure in the vortex-shedding case is disproportionally high, in comparison with the increase in Reynolds number. This underlines the fact that in the vortex-shedding regime, new mechanisms of shear-related cell stress can develop, associated with the complex fluid particle (and advected cell) motion, caused by the chaotic saddle, which forms in the wake (for more detail, see Koynov and Khinast, 2004). We also computed dimensionless mean stress level rates and they are $6 \cdot 10^{-8}$ for the Re=8 case, $7.5 \cdot 10^{-8}$ for the Re=42 case and $1.1 \cdot 10^{-7}$ for the Re=68 case. It is important to realize that the reported times in Figure 4 are of the order of several seconds and that the cell stress level caused by the bubble motion over these periods is minimal. Nevertheless, over extended periods of time the cumulated cell stress may impact viability and productivity, and Fig. 4 is helpful in understanding the effects of different bubble types.

Another way of quantifying the shear exposure of suspended cells in different bubble wakes is to study the distribution of cells, which have sustained a certain cumulative cell stress level as a fraction of the total number of cells (as shown in Figure 5 for the three single-bubble cases). In this graph, cell stress levels are plotted on the x-axis and the fraction of cells, having sustained a certain amount, can be found on the y-axis. All three curves have maxima near the origin, which suggests that most cells have been exposed to minimal levels of shear. The fraction of cells potentially sustaining higher damage drops quickly, as the areas of the computational volume, where high shear occurs are very small. While the low and intermediate Reynolds number cases yield distributions, which

are very similar (with a large portion of the cells remaining unaffected, as can be inferred from the fact that the maximum of the peak is at the zero stress level), the vortex-shedding cases differ in the fact that all cells are exposed to a certain amount of cumulative shear (the fraction of cells that have sustained a total level between 0 and $1 \cdot 10^{-8}$ is zero). This is caused by the motion of the vortices (and their subsequent interaction with following bubbles), which extends the influence of the rising bubble to the entire computational domain. The peak in this case is also lower (with a smaller area under the curve, indicating fewer cells having been exposed to a certain amount of shear), proving that the low shear zone on the sides of the main wake is narrower (the narrower the wake, the wider the low shear zone, the higher the fraction of cells suffering low levels of shear exposure). Overall, it can be concluded that in the case of single rising bubbles, the cell stress sustained by suspended animal cells in vortex-shedding wakes is significantly higher than in steady wakes.

It is well known that the bubbly gas-liquid flows in industrial reactors can exhibit several distinct regimes (Deckwer, 1992). Depending on the superficial gas velocity, bubbles can either rise in the so called homogeneous (or bubbly) regime, characterized by straight trajectories and minimal bubble-bubble interactions or in the heterogeneous (churn-turbulent) regime in which bubbles follow irregular paths and bubble break-up and coalescence are very common. While the assumption of bubbles rising alone is valid for homogeneous flows, it no longer applies for transitional and heterogeneous flows. Unless the superficial gas velocity is kept very low, bubbles can no longer be considered as rising alone, since the proximity of other bubbles has the potential to affect both their motion and the dynamics of the liquid flow around them. The transition between the two regimes depends on the geometry of the reactor and viscosity of the medium, among other factors, with higher viscosities usually enhancing the transition (Ruzicka et al., 2003). In order to account for the changes in the continuous-phase hydrodynamics due to bubble-bubble interactions (Dhanasekharan et al., 2005), multiple bubbles were considered in our simulations.

Figure 6 shows snapshots of the cumulative stress level fields (as they develop over time) for cells suspended around three bubbles rising simultaneously. Flows at both low and

high Reynolds number are considered. In the low-Reynolds-number case, the bubbles initially move laterally, as well as vertically for a very short period of time, until an equidistant configuration is achieved. From this point on, they rise, much like single bubbles, in straight trajectories, with steady wakes (and high shear rates observed only in the wake regions). This is an example of bubble-bubble interactions being too weak to influence the bubble motion. The opposite is observed in the case of the high-Reynolds-number flows. Intense bubble-bubble interactions cause bubbles to slow down or accelerate, and to move laterally as well as vertically in trajectories, which differ significantly from the single-bubble case. In this flow, the shear stresses affecting the suspended cells are distributed almost uniformly over the entire computational domain.

At higher gas volume fractions, bubble-bubble interactions become strong enough to influence even low-Reynolds-number flows. The ensuing cumulative shear-related cell stress level is shown in Figure 7 for nine bubbles of two different Reynolds numbers. While the bubbles start off moving in parallel trajectories, wake interactions cause some of them to accelerate and others to fall behind. These interactions also help destroy the symmetry of the bubbles' wakes, resulting in a wavy, meandering bubble motion. Fluid stretching and folding can be significant sources of liquid phase shear. It can be seen that, while cells are exposed to roughly uniform levels of shear throughout the flow around the nine bubbles rising in the low Reynolds number case, low fluid stretching and folding keep the actual magnitude of this exposure relatively low. This is not the case in the high-Reynolds-number flow. The lamellar structures formed by fluid element stretching and folding occurring due to the chaotic mixing become visible, brought out by the high associated cumulative cell damage. The magnitude of the shear stresses, to which cells in these zones of intense mixing are subjected, is significantly higher than in the low Reynolds number case.

Figure 8, showing two snapshots of the shear stress fields around nine bubbles rising at a low and high Reynolds number, provides further insight in the nature of the shear generating phenomena. From Fig. 8a, it can be seen that, even though the symmetry between the recirculation zones in the low Reynolds number wakes is destroyed

(resulting in non-linear motion), the actual zones still exist and are the predominant sources of shear. In the high Reynolds number case, vortices are still shed by the bubbles (or groups of bubbles behaving as a single large bubble). However, additional, independent high-shear vortical structures persist throughout the entire domain. These shear field differences indicate that there still exists a fundamental difference between the mechanisms of mixing in recirculating and vortex-shedding wakes (similar to the one outlined for the case of single bubbles in Koynov and Khinast, 2004).

The correlation between liquid-phase mixing and suspended cell shear exposure can also be seen in Figure 9, which shows the average cumulative stress level as a function of time. It is not surprising that the cells in the nine-bubble, high Reynolds number case potentially suffer higher damage and stress. It is noteworthy, however, that the average cell stress level in the three-bubble, high-Reynolds-number case also exceeds the one observed in the nine-bubble, low-Reynolds-number case. This result indicates that the shear generating potential of chaotic mixing *significantly exceed that* of the shear flows observed in steady wakes. This conclusion is further supported by Figure 10, which shows the distribution of cells having sustained a certain amount of cumulative stress level as a fraction of the total number of cells. The peak, corresponding to the nine-bubble, high-Reynolds-number case is farthest to the right, denoting highest amount of shear exposure, but it is also the widest, which signifies that the highest fraction of all cells throughout the computational domain have been exposed to it. The similarities between the peaks corresponding to the high-Reynolds-number three-bubble case and the low-Reynolds-number nine-bubble case can be explained by Figures 6 and 7. It can be seen that in the beginning of their ascent, the nine bubbles form three loose clusters (each consisting of three bubbles), which behave like large individual bubbles, (i.e., three bubbles rising at a high Reynolds number). After some time, these clusters are destroyed, which corresponds to the inflection point in the average shear exposure graph.

4.3 Oxygen supply

From our simulations it is evident that liquid-phase mixing has an impact on suspended cell viability. Efficient dissolved oxygen transport, however, is dependent on good

mixing and oxygen deprivation can also damage the cells over prolonged periods of time. In order to investigate the differences in the oxygen supply to suspended cells in different flows, numerical simulations of oxygen interfacial mass transfer, liquid-phase transport and oxygen consumption by the cells were performed. These simulations are capable of replicating the realistic behavior of the systems considered, as can be seen in Figure 11. Figure 11a shows the dissolved oxygen concentration field behind a bubble rising in the vortex-shedding regime, as obtained using Laser Induced Fluorescence techniques by Bork et al., (2003). Figure 11b and c shows our numerical results (stream traces and dissolved oxygen concentration) for the same case. It can be seen that there is a very good agreement between the two. This figure also provides a very good visual example of the mechanism of mass transport in a vortex-shedding wake. It can clearly be seen that as oxygen transfers phase at the bubble interface, it is quickly transported away by the shedding vortices.

The differences in the mechanisms of dissolved oxygen transport are better illustrated in Figure 12, which shows the average hypoxia-induced cell stress level as a function of time for a single bubble rising at a low, intermediate and high Reynolds number. It can be seen that, while the low and intermediate Reynolds number cases show a steady rate of potential damage, the accumulative damage reaches a plateau in the vortex-shedding case, as the vortex shedding bubble effectively delivers oxygen to the whole domain.

Oxygen transport from multiple bubbles was considered as well, and the results are shown in Figure 13 (sample snapshots of the dissolved oxygen concentration fields are shown in Fig. 14). It can be seen, that in all cases, the stress level accumulation reaches an asymptotic constant value for the cell densities and oxygen consumption simulated. In all cases, the supply of oxygen far exceeds the consumption, resulting in adequate aeration throughout the domain. Slight cell damage occurs only initially, when bubbles start to rise. Thus, it can be concluded that cell stress levels due to hypoxia is *not a micro-phenomenon* in bioreactors. Large-scale mixing problems, where some parts of a reactor are not properly aerated are *thus the cause of any hypoxia damage*.

The cell densities used for this study, while within the range used in bioreactors, are relatively low. In many industrial tanks, values several orders of magnitude higher are considered. In such tanks, oxygen consumption will be higher and so will be the possibility that oxygen transport becomes a limiting factor. This will be the topic of further studies.

5 Conclusions

Detailed high-resolution simulations were performed describing mammalian cells suspended in a liquid phase through which air bubbles rise (approximating the conditions in the bulk of sparged bioreactors). The objective was to study the local shear environments in bubbly flows, characterized by different parameters, such as gas hold-up as well as bubble Reynolds, Morton and Eötvos numbers. Knowledge of the local shear stresses was then used to asses the cumulative stress levels that suspended cells would sustain over time. Additionally, the resolution of the local liquid-phase velocities allows the study of the interfacial mass transfer of oxygen and its subsequent transport in the liquid phase. The main conclusions of our work are:

- The hydrodynamics of bubbly flows differ significantly as a function of operating conditions and so do the ensuing cell damaging shear forces. At low Reynolds numbers (as long as the bubble wake remains steady), the high-shear zone is confined to the bubble wake and the actual magnitude of the stresses, which is relatively low, is mostly independent of the Reynolds number. As soon as the bubble enters the vortex-shedding regime, both the magnitude of the local shear stresses and the size of the high shear zones sharply increase, and with them – the potential of cell damage. In addition, shear stresses dominate normal stresses. However, their relative potential to inflict cell stress needs to be evaluated in the future.
- In the case of bubble swarms, even at low Reynolds numbers, the bubbles move in meandering trajectories, extending the high-shear zone (which in single bubble cases is confined to the narrow region surrounding the bubble's linear path) over the entire domain. However, even in large swarms, low-Reynolds-number flows result in significantly lower cumulative shear exposure than the higher Reynolds

number flows. This difference is due to the intense chaotic mixing observed almost exclusively in high-Reynolds-number flows and caused by the chaotic saddles created by the periodic vortex shedding phenomenon.

- While it is known that good liquid-phase mixing significantly improves the dissolved oxygen transport to the cells and can prevent hypoxia-related damage, for the cell concentrations considered in this study, oxygen consumption by the cells was too low and transport effects were only seen in the single bubble cases. It was shown that the increase in DO quantities resulting from the increase in gas volume fraction associated with an increase in the number of rising bubbles far outstrips the differences caused by the mixing disparities between the different flows. Therefore, an obvious conclusion is that oxygen supply problems in bubbly flows are better addressed by increasing the gas hold-up, than by improving the liquid-phase mixing. Also, oxygen supply is a macro-phenomenon and not a micro-effect in the reactor.

The results of the hydrodynamics and cell transport and shear exposure simulations suggest that lower Reynolds number flows will be less harmful to the suspended cells, due to lower rates of shear stress generation. However, it is important to emphasize the fact that this study only considers the local flow dynamics in the bulk of the fluid phase and ignores the areas in the vicinity of the reactor walls and especially at the free surface. It has been shown that smaller bubbles result in harsher conditions for biological cells at the free surface in reactors (which is where most of the cell damage occurs). The current study cannot, therefore, be used as a comprehensive tool for the design of bioreactors. It should rather be seen as an application of state of the art numerical simulations to a previously unaddressed problem, the results of which can be applied towards a further understanding of all phenomena involved in complex multiphase systems, such as bioreactors and can help the future “fine tuning” of their operation.

6 Future work

On of the subjects of future work will be the modeling of bubbles rising to free surfaces and the resulting cell damage. Another objective will be the analysis of species transport.

Dissolved oxygen is not the only dissolved species that can affect cell suspensions in bioreactors. In the future, it is our intention to simulate nutrient supply and consumption as well as metabolic byproducts (lactic acid, CO_2) generation and removal. Additionally, apoptotic cells release cytokines, which can signal other, healthy cells to initiated programmed cell death. It is our opinion that the differences in flow fields and transport characteristics observed in different bubbly flows will have an impact on the action of this mechanism.

Acknowledgement: JGK gratefully acknowledges partial support of this work by NSF Grant CTS 02098764. We also want to thank the reviewer for their helpful suggestions regarding our cell damage modeling.

7 Notation

a_c	coefficient associated with the damage model, $N^{-2}m^4$
b_c	coefficient associated with the damage model, $N^{-1}m^2$
c_c	coefficient associated with the damage model
c_{hp}	dissolved oxygen concentration, below which hypoxia occurs, kmol/m^3
$c_{l,O2}$	concentration of species oxygen in the liquid phase, kmol/m^3
$c_{g,O2}$	concentration of species oxygen in the gas phase, kmol/m^3
D	deformation
D_b	deformation at bursting
D_{O2}	dissolved oxygen diffusion coefficient in the liquid phase, m^2/s
d_b	equivalent circle diameter of the bubble, m
d_c	coefficient associated with the hypoxia damage model
Eo	Eötvos number, $Eo = g\rho_l d_b^2 / \sigma$
f	body forces, N
g	gravitational acceleration, m/s^2
H	Heaviside function
H_c	hypoxia damage
k_L	liquid-side mass transfer coefficient, m/s
Mo	Morton number, $Mo = g\mu_l^4 /(\rho_l \cdot \sigma^3)$
P	pressure, Pa
Pe	Peclet number, $Pe = U_t d_b / D$
r_b	oxygen consumption rate, kmol/m^3·s
r_c	cell radius, m
Re_b	bubble Reynolds number, $\mathrm{Re}_b = d_b U_t \rho_l / \mu_l$
Sc	Schmidt number, $Sc = \mu /(\rho \cdot D)$
Sh	Sherwood number, $Sh = k_L d_b / D$
t	time, s
$\tilde{t}$	dimensionless time
u	velocity vector, m/s
$\mathbf{u}_c$	velocity of a cell, m/s
u_c	x-velocity component at the location of the cell, m/s
v_c	y-velocity component at the location of the cell, m/s
$\mathbf{u}_{i,j}$	velocity in the i,j-th cell, m/s
U_t	terminal rise velocity, m/s
$w_{i,j}$	weighing functions
We	Weber number, $We = d_b U^2{}_t \rho_l / \sigma$
x	position vector
x	x-coordinate
x'	x-coordinate of points lying inside the bubble interface
y	y-coordinate
y'	y-coordinate of points lying inside the bubble interface

Greek letters

κ	curvature
μ_l	liquid-phase viscosity, Pa·s
μ_i	viscosity inside the cell, Pa·s
ξ	Taylor coefficient
ρ_l	liquid-phase density, kg/m^3
ρ_g	gas-phase density, kg/m^3
ρ_i	density of i-th phase, kg/m^3
σ	bubble surface tension, N/m
σ_x	normal stress x-direction, N/m^2
σ_y	normal stress x-direction, N/m^2
σ_b	bursting membrane tension, N/m
σ_c	cell membrane tension, N/m
τ	shear stress, N/m^2
χ	cell stress level

8 References

Abu-Reesh, I. and Kargi, F., "Biological Responses of Hybridoma Cells to Defined Hydrodynamic Shear Stress", *Journal of Biotechnology*, **9**, (1989), 167-178.

Al-Rubeai, M., Emery, A. N., Chalder, S. and Goldman, M. H., "A flow cytometric study of hydrodynamic damage to mammalian cells" *J. Biotechnol.*, **31**, (1993), 161-177.

Al-Rubeai, M., Singh, R. P., Goldman, M. H., Emery, A. N., "Death mechanisms of animal cells in conditions of intense agitation", *Biotechnol*. *Bioeng.*, **45**, (1995) 463-472.

Al-Rubeai, M. and Singh, R., "Apoptosis in cell culture", *Current Opinion in Biotechnology*, **9**, (1998) 152-156.

Aris, R. Mass transfer from small ascending bubbles*. Chem. Eng. Sci*.1997; **52**: *4439-4446***.**

Arathoon, W. R. and Birch, J. R., "Large-scale cell culture in biotechnology." *Science*, **232**, (1986), 1390-1395.

Birch, J., Lambert, K., Thompson, P. W., Kenney, A. C. and Wood, L. A., "Antibody production with airlift fermentors.", in: Lydersen, B. K. (Eds.), Large Scale Cell Culture Technology, Hanser, New York, (1987)d 1-20.

Bork, O., M. Schlueter, S. Scheid, Raebiger N. Analysis of the effect of local hydrodynamics on mass transfer from bubbles using laser induced fluorescence. *Proceedings of FEDSM'03*. 2003. *1-7*.

Born, C., Zhang, Z., Al-Rubeai, M. and Thomas, C., "Estimation of Disruption of Animal Cells by Laminar Shear Stress", *Biotechnology and Bioengineering*, **40**, (1992), 1004-1010.

Bothe, D., Koebe, M., Wielage, K. and Hans-Joachim Warnecke. VOF simulations of mass transfer from single bubbles and bubble chains rising in aqueous solutions. Proceedings of FEDSM'03. 2003. *1-7*.

Boudrant, J., Menshutina, N., Skorohodov, A., Guseva, E., Fick, M., "Mathematical modeling of cell suspension in high cell density conditions. Application to L-lactic acid fermentation using *Lactobacillus casei* in membrane bioreactor", *Process Biochemistry*, **40**, (2005) 1641-1647.

Brackbill, J.U., D.B. Kothe, C. Zemach, A continuum method for modeling surface tension, J. Comput. Phys. 100 (1992) 335.

Camacho, F., Gomez, A., Sobczuk, T., Grima, E., "Effects of mechanical and hydrodynamic stress in agitated, sparged cultures of Porphyridium cruentum" *Process Biochemistry*, **35**, (2000), 1045-1050.

Chalmers, J. and Bavarian, F. "Microscopic visualization of insect cell-bubble interactions II: The bubble film and bubble rupture" *Biotechnol. Prog.*, **7**, (1991), 151-158.

Cheng, E.H.-Y., Kirsch, D.G., Clem, R.J., Ravi, R., Kastan, M.B., Bedi, A., Ueno, K., Hardwick, J.M., "Conversion of Bcl-2 to a Bax-like death effector by caspases." *Science,* **278**, (1997) 1966–1968.

Cherry, R.S. and Hulle, C.T. "Cell death in thin films of bursting bubbles", *Biotechnol. Prog*., **8**, (1992)11–18

Chisti, Y. and Moo-Young, M., "Disruption of microbial cells for intracellular products" *Enzyme Microb. Technol.*, **8**, (1986), 194-204.

Chisti, Y. "Animal cell culture in stirred bioreactors: observations on scale-up", *Bioprocess Eng*., **9**, (1993) 191–196

Chisti, Y., "Animal-Cell Damage in Sparged Bioreactors**",** *TIBTECH*, **18**, (2000).
Chisti, Y., "Hydrodynamic Damage to Animal Cells", *Critical Reviews in Biotechnology*, **21**, (2001) 67-110.

Chisti, Y., and Jauregui-Haza, U., "Oxygen transfer and mixing in mechanically agitated airlift bioreactors", *Biochem. Eng. Journal*, **10**, (2002) 143-153.

Choi, H. M., Kurihara, T., Monji, H., Matsui, G. Measurement of particle/bubble motion and turbulence around it by hybrid PIV. *Flow Measurement and Instrumentation*. 2002; **12**: *421-428***.**

W.D. Deckwer, "Bubble Column Reactors", Wiley, Chichester, 1992

Dey, D., Boulton-Stone, J. M., Emery A. N. and Blake, J. R., "Experimental comparisons with a numerical model of surfactant effects on the burst of a single bubble", *Chemical Engineering Science*, **52**, (1997) 2769-2783.

Dey, D, Emery, A. N., "Problems in predicting cell damage from bubble bursting", *Biotechnol Bioeng.*, **65(2)**, (1999) 240-245.

Dimmler, S., Haendeler, J., Rippmann, V., Nehls, M., Zeiher, A. M., „Shear stress inhibits apoptosis of human endothelial cells", *FEBS Lett*, **398**, (1996) 71-74.

Dhanasekharan, K. M., Sanyal, J., Jain A., and Haidari, A., "A generalized approach to model oxygen transfer in bioreactors using population balances and computational fluid dynamics", *Chemical Engineering Science*, **60**, (2005), 213-218.

Emery, A. N., Jan, D., Al-Rubeai, M., "Oxygenation of intensive cell-culture systems", *Appl. Microbiol. Biotechnol.*, **43**, (1995) 1028-1033.

Fadeel, B., Zhivotovsky, B., Orrenius, S., "All along the watchtower: on the regulation of apoptosis regulators." *FASEB J.,* **13**, (1999) 1647–1657.

Fedkiw, R., and Osher, S., "Level set methods: An overview and some recent results", J. Comput. Phys. 169 (2001) 463.

Garcia-Briones, M. and Chalmers, J., "Flow parameters associated with hydrodynamic cell injury", *Biotechnol. Bioeng.*, **44**, (1994), 1089-1098.

Gregoriades, N., Clay, J., Ma, N., Koelling, K., Chalmers, J., "Cell damage of microcarrier cultures as a function of focal energy dissipation created by a rapid extensional flow", *Biotechnol. Bioeng*., **69**, (2000)

Glimm, J. W. Grove, X. L. Li, W. Oh, and Sharp D. H. A critical analysis of Rayleigh–Taylor growth rates. *J. Comput. Phys*. 2001; **169**: *652-677***.**

Grima, E., Chisti, Y. and Moo-Young, M., "Characterization of shear rates in airlift bioreactors for animal cell culture", *J. Biotechnol.*, **54**, (1997), 195-210.

Guo, X. Y., Rathor, M, N., Ti, H., C., "Hydrodynamics and mass transfer studies in a novel external-loop airlift reactor" *Chem. Eng. J.*, **67**, (1997), 205-214.

Hand-Corrigan, A., Emery, A. N. and Spier, R. E., "Effect of gas-liquid interfaces on the growth of suspended mammalian cells; Mechanisms of cell damage by bubbles" *Enzyme Microbial Tecnology*, **11**, (1989), 230-235.

Handa, A, Emery, A. N., Spier, R. E., "On the evaluation of gas–liquid interfacial effects on hybridoma viability in bubble column bioreactors", *Dev. Biol. Stand*. **66**, (1987) 241–253

Hu, W.-S. and Aunins, J., "Large-scale mammalian cell culture", *Current Opinion in Biotechnology*, **8**, (1997) 148-153.

Illing, S. and Harrison, T. L., "The kinetics and mechanism of Corynebacterium glutamicum aggregate breakup in bioreactors" *Chem. Eng. Science*, **54**, (1999), 441-454.

Jobses, I., Martens, D., Tramper, J., "Lethal events during gas sparging in animal cell Culture", *Biotechnol. Bioeng.*, **37** (1991) 476-483.

Jung, C., T. Tel, E. Ziemniak, "Application of Scattering Chaos to Particle Transport in a Hydrodynamical Flow", *Chaos*, **4**, 555 (1993).

Jung J. Y., Park J. K., Chang, H. N.,"Bacterial cellulose production by *Gluconacetobacter hansenii* in an agitated culture without living non-cellulose producing cells", Enzyme and Microbial Technology, **37**, (2005) 347–354.

Koynov, A. and Khinast, J. effects of hydrodynamics and Lagrangian transport on chemically reacting bubble flows. *Chem. Eng. Sci*. 2004; **59**: *3907-3927*.

Kunas, K. T. and Papoutsakis, E. T., "Damage mechanisms of suspended animal cells in agitated bioreactors with and without bubble entrainment" *Biotechnol. Bioeng.*, **36**, (1990), 476-483.

Lakehal, D., Meier, M. Fulgodi, M., „Interface tracking towards the direct simulation of heat and mass transfer in multiphase flows", *International Journal of Heat and Fluid Flow*, **23**, (2002) 242-257.

Legendre, D., Magnaudet, J. Effect of flow acceleration on mass or heat transfer at the surface of a spherical bubble. *C. R. Acad. Sci. Paris*. 1999; **327**: *63-70***.**

Lubiniecki, A. S. Ed., "Large-Scale Mammalian Cell Culture Technology", Dekker, New York, (1990).

Martens, D. E., de Gooijer, C. D., Beuvery, E. C., Tramper, J., "Effect of serum concentration on hybridoma viable cell density and production of monoclonal antibodies in CSTRs and on shear sensitivity in air-lift loop reactors", *Biotechnol. Bioeng*., **39**, (1992) 891-897.

Meier, S. J., Hatton, T. A., Wang, D. I., "Cell death from bursting bubbles: role of cell attachment to rising bubbles in sparged reactors", *Biotechnol. Bioeng*., **62**, (1999) 468–478

Millies, M., and Mewes D. Calculation of circulating flows in bubble columns. *Chem. Eng. Sci.* **50,** 1995 2093-2106.

Mollet, M., Ma, N., Zhao, Y., Brodkey, R., Taticek, R., Chalmers, J. "Bioprocess Equipment: Characterization of Energy Dissipation Rate and its potential to Damage Cells", *Biotechnology Progress* **20,** (2004) 1437-1448.

Oh, S.K.W., Nienow, A.W., Al-Rubeai, M., Emary, A.N., "The effect of agitation intensity with and without continuous sparging on the growth and antibody production of hybridoma cells", *J. Biotechnol.*, **12**, (1989) 45-62.

Perani, A., Singh, R. P., Chauhan, R., Al-Rubeai, M., "Variable functions of bcl-2 in mediating bioreactor stress-induced apoptosis in hybridoma cells", *Cytotechnology*, **28**, (1998) 177-188.

Proskuryakov, S., Konoplyannikov, A. and Gabai, V., "Necrosis: a specific form of cell death?" *Experimental Cell Research*, **283**, (2003) 1-16.

Ramirez, O. T. and Mutharasan, R., "Effect of serum on the plasma membrane fluidity of hybridomas: An insight into its shear protective mechanism.", *Biotechnol. Rog.*, **8**, (1992), 40-50.

Raymond, F., Rosant, J.-M. A numerical and experimental study of the terminal velocity and shape of bubbles in viscous liquids. *Chem. Eng. Sci*. 2000; **55**: *943-955***.**

Ruzicka, M. C., Drahos, J., Mena, P. C. and Teixeira, J. A., "Effect of viscosity on homogeneous-heterogeneous flow regime transition in bubble columns", *Chemical Engineering Journal*, **96**, (2003), 15-22.

Sankaranarayanan, K., Kevrekidis, I. G., Sundaresan, S., Lu, J. and Tryggvason, G. A comparative study of lattice Boltzmann and front-tracking finite-difference methods for bubble simulations. *International Journal of Multiphase Flow*. 2003; **29**: *109-116***.**

Scardovelli, R. and Zaleski S. "Direct numerical simulation of free-surface and interfacial flow". *Annu. Rev.Fluid Mech*. 1999, **31**: *567-603*.

Shopov, P. J.,Minev, P. D., Bazhekov, I. B. and Zapryanov Z. D. "Interaction of a deformable bubble with a rigid wall at moderate Reynolds numbers". *J. Fluid Mech.* 1990; **219**: *241 - 271***.**

Silva-Santisteban B. O., Y´epez, Filho, F. M., "Agitation, aeration and shear stress as key factors in inulinase production by *Kluyveromyces marxianus*", Enzyme and Microbial Technology, **36,** (2005) 717–724.

Simpson, N. H., Milner, A. N., Al-Rubeai, M., "Prevention of hybridoma cell death by bcl-2 during sub-optimal culture conditions", *Biotechnol. Bioeng.*, **54**, (1997) 1-16.

Singh, V., "Disposable bioreactor for cell culture using wave-induced agitation", *Cytotechnology,* **30**, (1999), 149-158.

Sowana, D.D., Williams, D.R.G., O'Neill, B.K., Dunlop, E.H., "Studies of the shear protective effects of Pluronic F-68 on wild carrot cell cultures", Biochemical Engineering Journal, **12**, (2002) 165–173.

Taylor, G. I., ''The Formation of Emulsions in Definable Fields of Flow,'' *Proc*. *Roy*. *Soc*. *A*, **146**, (1934) 501-1934.

Tintó, A., Gabernet, C., Vives, J., Prats, E., Cairo´ , J.J., Cornudella, L., Go` dia, F., "The protection of hybridoma cells from apoptosis by caspase inhibition allows culture recovery when exposed to noninducing conditions." *J. Biotechnol.*, **95**, (2002) 205–214.

Tokuhiro, A., Maekawa, M., Iizuka, K., Hishida, K., Maeda, M. Turbulent flow past a bubble and an ellipsoid using shadow-image and PIV techniques. *International Journal of Multiphase Flow*. 1998; **24**: *1383-1406***.**

Tramper, J., Joustra, D. and Vlak, M. "Bioreactor design for growth of shear-sensitive insect cells: In: Webb, C. and Mavintune, F. (Eds.), Plant and Animal cell Cultures: Process Possibilities, Ellis Horwood, Chichester, UK, (1987), 125-136.

Tramper, J., Smith, J. D., Sreaatman, J., Valk, J. M., "Bubble-column design for growth of fragile insect cells", *Bioprocess Engin.*, **3,** (1988) 37-41.

Tryggvason, G., B. Bunner, A. Esmaeeli, D. Juric, N. Al-Rawahi, W. Tauber, J. Han, S. Nas and Y. Jan, "A Front-Tracking Method for the Computations of Multiphase Flow", *Journal of Computational Physics*, **169**, (2001).

van der Pol, L. A., Beeksma, I. and Tramper, J., "Polyethylene glycol as protectant against damage caused by sparging for hybridoma suspension cells in a bubble column", *Enzyme Microb. Technol.*, **17**, (1995), 401-407.

van Wachem, B. G. M. and Schouten, J. C. Experimental validation of a 3D Lagrangian VOF model: shape and rise velocity. *AIChE Journal*. 2002, **48**: *2744-2753***.**

Vives, J., Juanola, S., Cairo, J., Godia, F., "Metabolic engineering of apoptosis in cultured animal cells: implications for the biotechnology industry", *Metabolic Engineering*, **5**, (2003) 124-132.

Wu, J., "Mechanisms of animal cell damage associated with gas bubbles and cell protection by medium additives" *Journal of Biotechnology*, **43**, (1995), 81-94.

Ziegelstein, P. C., Chen, L., Caprogossi, M. C., "Flow-dependent cytosolic acidification of vascular endothelial cells." *Science*, **258**, (1992), 656-659.

Zhang, Z., Ferenczi, M. A. And Thomas, C. R., "A micromanipulation technique with a theoretical cell model for determining mechanical properties of single mammalian cells", *Chem. Eng. Science*, **47**, (1992), 1347-1354.

Zhang, Z., Chisti, Y. and Moo-Young, M., "Effects of the hydrodynamic environment and shear protectants on survival of erythrocytes in suspension." *J. Biotechnol.*, **43**, (1995), 33-40.

9 Tables

Table I. Values of the dimensionless numbers describing the system.

Table II. Values of coefficients used in the damage model.

Figures

Figure 1. Stream traces associated with the velocity fields in the liquid phase past rising bubbles a.) Single bubble in the steady wake regime (Re=8, Eö=3.125, Mo=$1.2\cdot10^{-3}$), b.) Single bubble in the vortex-shedding regime (Re=68, Eo=3.125, Mo=$5\cdot10^{-7}$), c.) Nine bubbles (Re_{av}=12, Eö=3.125, Mo=$1.2\cdot10^{-3}$), d.) Nine bubbles (Re_{av}=75, Eo=3.125, Mo=$5\cdot10^{-7}$).

Figure 2a. Shear stress fields around single rising bubbles (blue –low, red-high) for a) Re=8, $\tilde{t}$=25; b) Re=68, $\tilde{t}$=25; c) Re=8, $\tilde{t}$=100 and d) Re=68, $\tilde{t}$=100.

Figure 2b. Cumulative fraction of computational cells with stress components $|\sigma_x|$, $|\sigma_y|$ and $|\tau|$ equal or smaller than a given value for two developed flow fields around nine rising bubbles: a) Re_{av}=12, $\tilde{t}$=75, b) Re_{av}=75, $\tilde{t}$=75.

Figure 3. Snapshots of shear-induced stress level of cells around single rising bubbles (Red – high damage, blue – low damage) at different times for a) Re=8, $\tilde{t}$=25; b) Re=8, $\tilde{t}$=100; c) Re=42, $\tilde{t}$=100; d) Re=68, $\tilde{t}$=25; e) Re=68, $\tilde{t}$=50 and f) Re=68, $\tilde{t}$=100.

Figure 4. Average shear-induced cell stress level with time for different individual bubble flow cases.

Figure 5. Fraction of cells having been exposed to a certain amount of stress at time ($\tilde{t}$=75) in the liquid flow past single rising bubbles.

Figure 6. Snapshots of shear-induced stress level of cells around three bubbles rising simultaneously (Red – high damage, blue – low damage) at different times for a) Re_{av}=8, $\tilde{t}$=25; b) Re_{av}=8, $\tilde{t}$=50; c) Re_{av}=8, $\tilde{t}$=100; d) Re_{av}=70, $\tilde{t}$=25; e) Re_{av}=70, $\tilde{t}$=50 and f) Re_{av}=70, $\tilde{t}$=100.

Figure 7. Shear-induced stress level cells around nine bubbles rising simultaneously (Red – high damage, blue – low damage) at different times for a) Re_{av}=12, $\tilde{t}$=25; b) Re_{av}=12, $\tilde{t}$=50; c) Re_{av}=12, $\tilde{t}$=100; d) Re_{av}=75, $\tilde{t}$=25; e) Re_{av}=75, $\tilde{t}$=50 and f) Re_{av}=75, $\tilde{t}$=100.

Figure 8. Shear stress fields around multiple rising bubbles (blue –low, red-high) for a) Re_{av}=12, $\tilde{t}$=100 and b) Re_{av}=75, $\tilde{t}$=100.

Figure 9. Average shear-induced cell stress level with time for different bubble cluster flow cases.

Figure 10. Fraction of cells having been exposed to a certain amount of shear stress in the liquid flow past rising bubble clusters at time ($\tilde{t}$=75).

Figure 11. a.) LIF image of the oxygen concentration field around a bubble rising in the vortex-shedding regime in a viscous solution (brightness decrease with increasing oxygen concentration) *Bork et al., (2003)*, b.) Stream-traces associated with the velocity field

around a bubble rising in the vortex-shedding regime (Re=68), c.) Numerically obtained dissolved oxygen concentration (Re=68, Sc=60).

Figure 12. Average hypoxia-induced cell damage with time for different individual bubble flow cases.

Figure 13. Average hypoxia-induced cell damage with time for different bubble cluster flow cases.

Figure 14. Numerically obtained dissolved oxygen concentration a.) Re=8, Sc=420, 3 bubbles; b.) Re=70, Sc=60, 3 bubbles; c.) Re=12, Sc=280, 9 bubbles; d.) Re=75, Sc=56, 9 bubbles.

Dimensionless number	Values
Re_b	8 - 68
Sc_i	62 - 431
Pe	3448 - 4216
We	1.3 - 3.0
Mo	$5 \cdot 10^{-7}$-$1.2 \cdot 10^{-3}$
Eo	3.125-8.0

Table I. Values of the dimensionless numbers describing the system.

Coefficient	Value
a_c	$5 \cdot 10^{-10}$ $N^{-2}m^4$
b_c	$6 \cdot 10^{-7}$ $N^{-1}m^2$
c_c	0.0017
c_{hp}	$1 \cdot 10^{-12}$kmol/m^3
d_c	$1.8 \cdot 10^{-6}$
r_b	$1 \cdot 10^{-12}$ mol/cell·s
D_b	0.5

Table II. Values of coefficients used in the damage model.

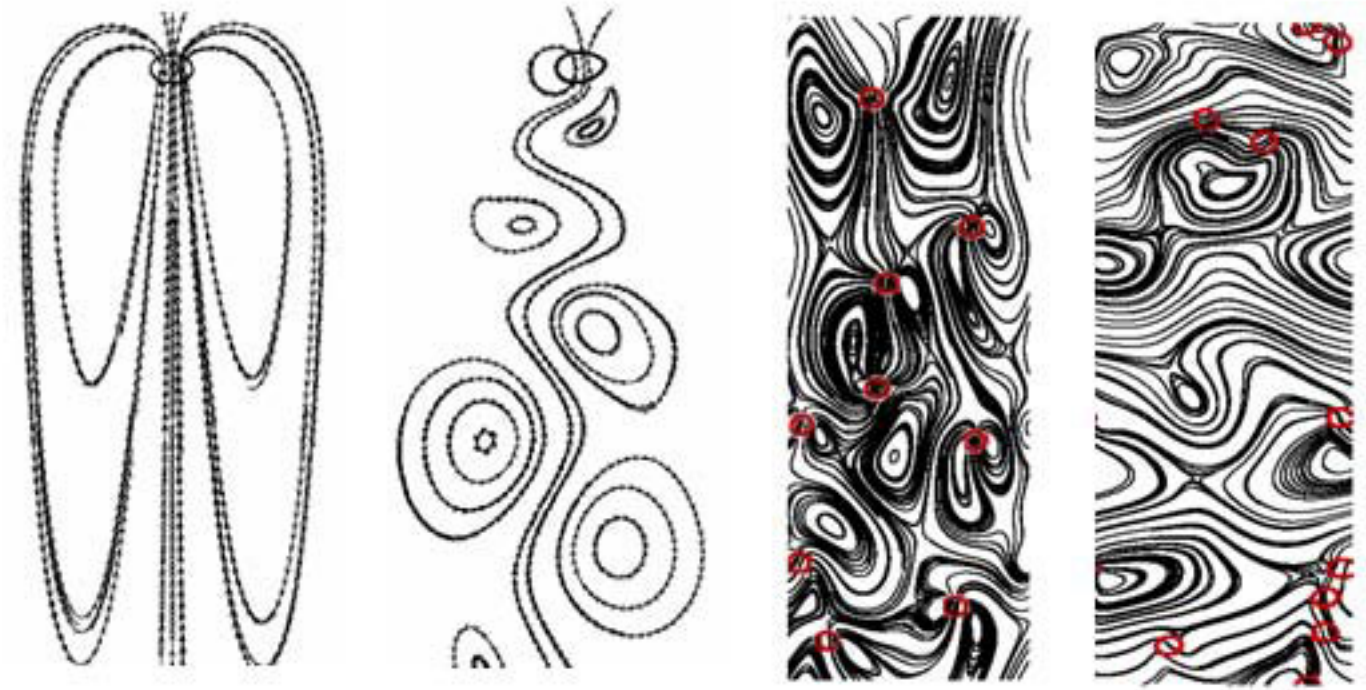

Figure 1. Stream traces associated with the velocity fields in the liquid phase past rising bubbles a.) Single bubble in the steady wake regime (Re=8, Eö=3.125, Mo=$1.2\cdot10^{-3}$), b.) Single bubble in the vortex-shedding regime (Re=68, Eo=3.125, Mo=$5\cdot10^{-7}$), c.) Nine bubbles (Re_{av}=12, Eö=3.125, Mo=$1.2\cdot10^{-3}$), d.) Nine bubbles (Re_{av}=75, Eo=3.125, Mo=$5\cdot10^{-7}$**).**

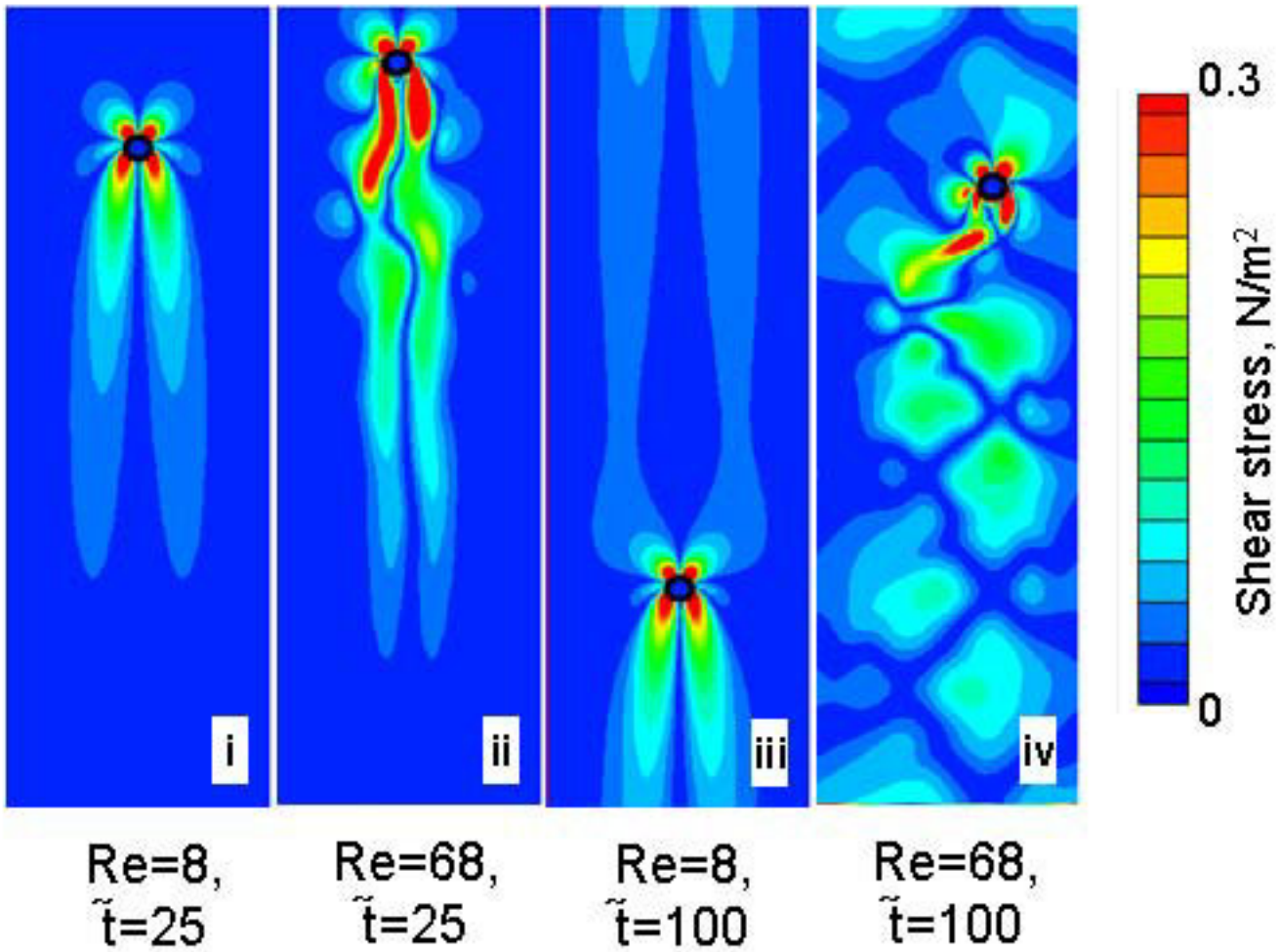

Figure 2a. Shear stress fields around single rising bubbles (blue–low, red-high) for i) Re=8, $\tilde{t}$=25; ii) Re=68, $\tilde{t}$=25; iii) Re=8, $\tilde{t}$=100 and iv) Re=68, $\tilde{t}$=100.

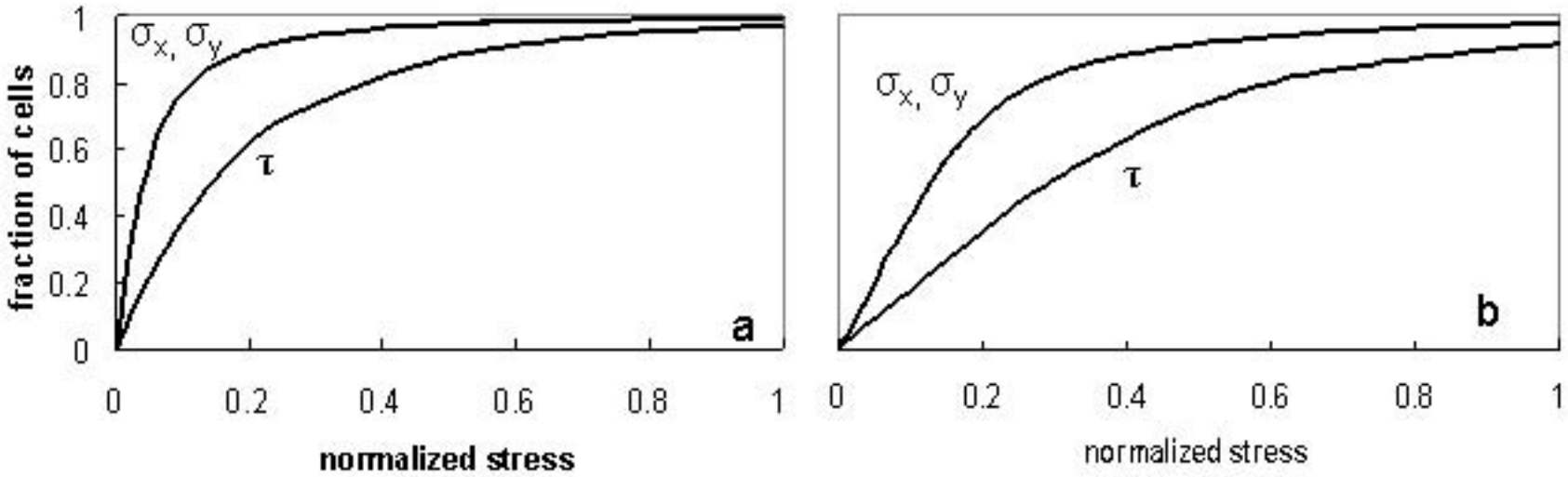

Figure 2b. Cumulative fraction of computational cells with stress components $|\sigma_x|$, $|\sigma_y|$ and $|\tau|$ equal or smaller than a given value for two developed flow fields around nine rising bubbles: a) $Re_{av}=12$, $\tilde{t}=75$, b) $Re_{av}=75$, $\tilde{t}=75$

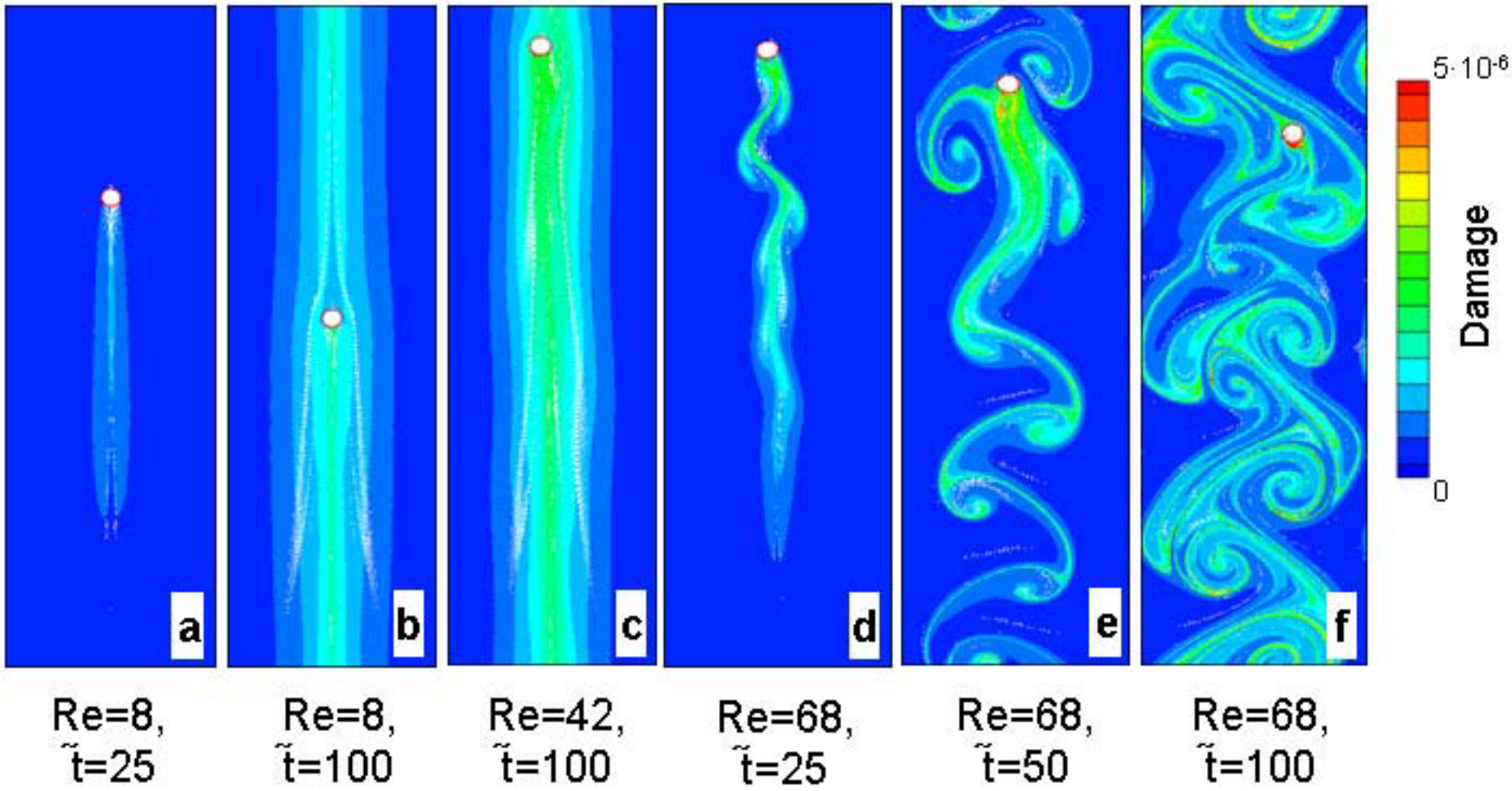

Figure 3. Snapshots of shear-induced stress level of cells around single rising bubbles (Red – high damage, blue – low damage) at different times for a) Re=8, $\tilde{t}$=25; b) Re=8, $\tilde{t}$=100; c) Re=42, $\tilde{t}$=100; d) Re=68, $\tilde{t}$=25; e) Re=68, $\tilde{t}$=50 and f) Re=68, $\tilde{t}$=100.

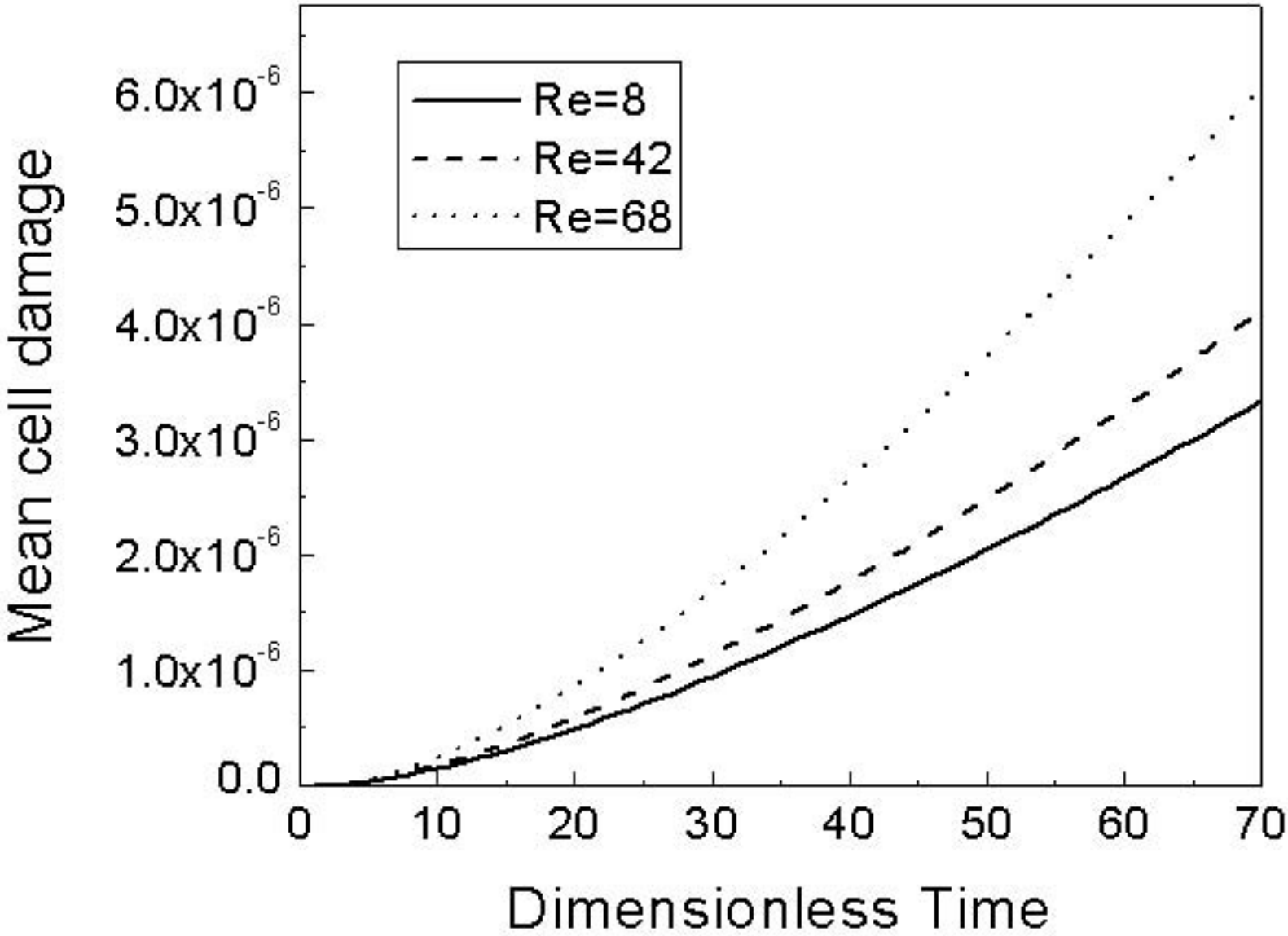

Figure 4. Average shear-induced cell stress level with time for different individual bubble flow cases.

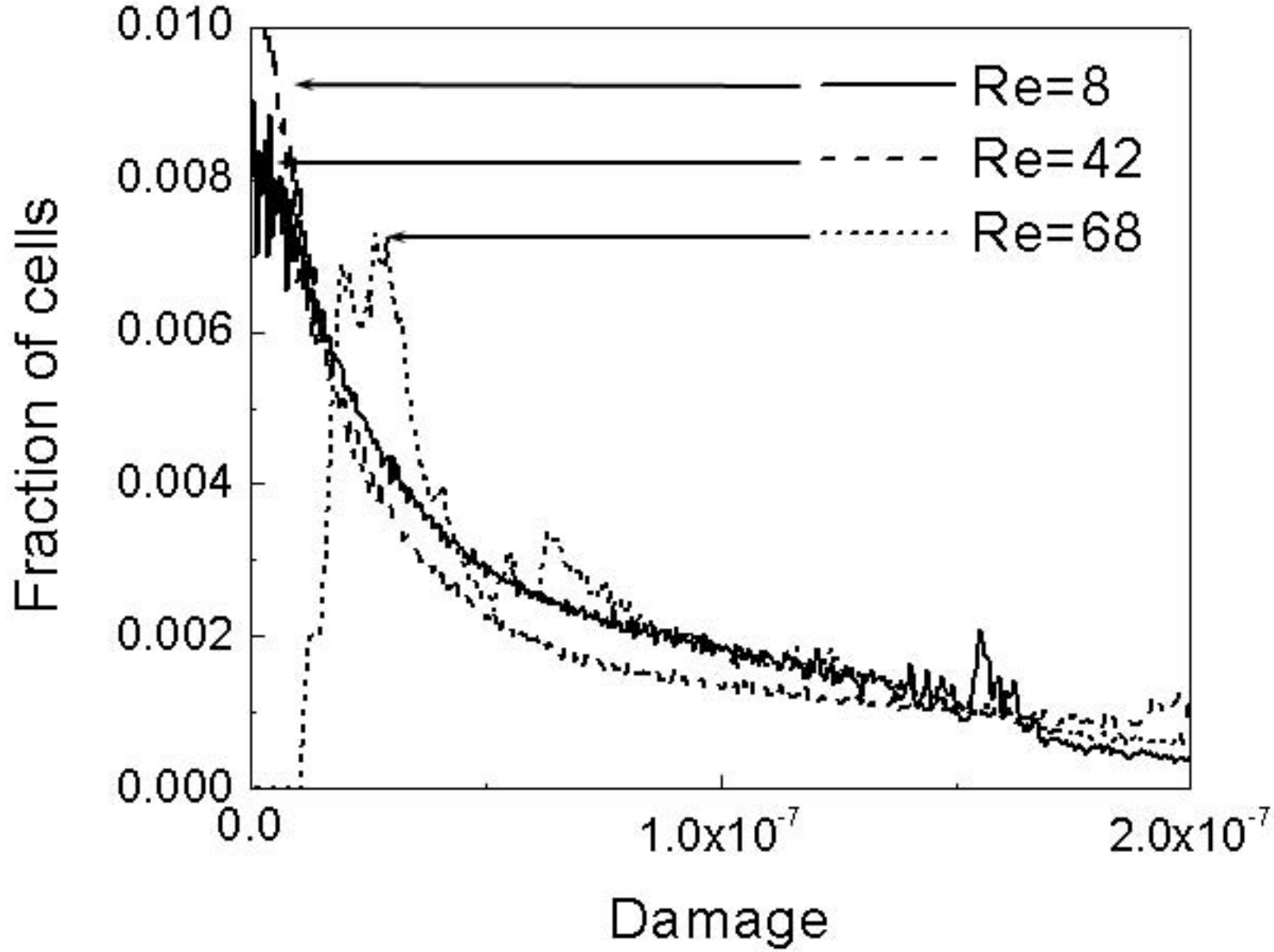

Figure 5. Fraction of cells having been exposed to a certain amount of stress at time ($\tilde{t}$=75) in the liquid flow past single rising bubbles.

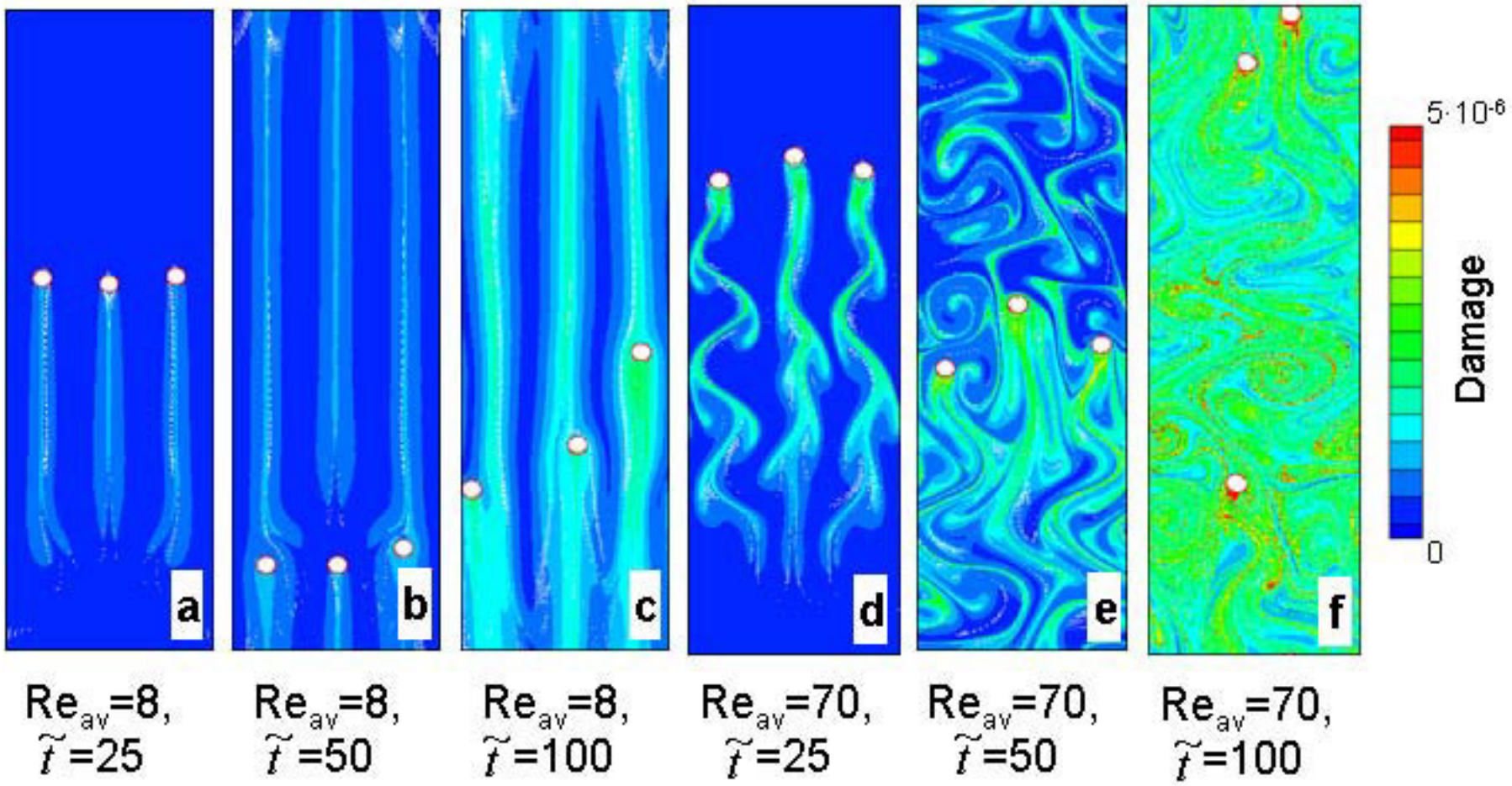

Figure 6. Snapshots of shear-induced stress level of cells around three bubbles rising simultaneously (Red – high damage, blue – low damage) at different times for a) Re_{av}=8, t=25; b) Re_{av}=8, $\tilde{t}$=50; c) Re_{av}=8, $\tilde{t}$=100; d) Re_{av}=70, $\tilde{t}$=25; e) Re_{av}=70, $\tilde{t}$=50 and f) Re_{av}=70, $\tilde{t}$=100.

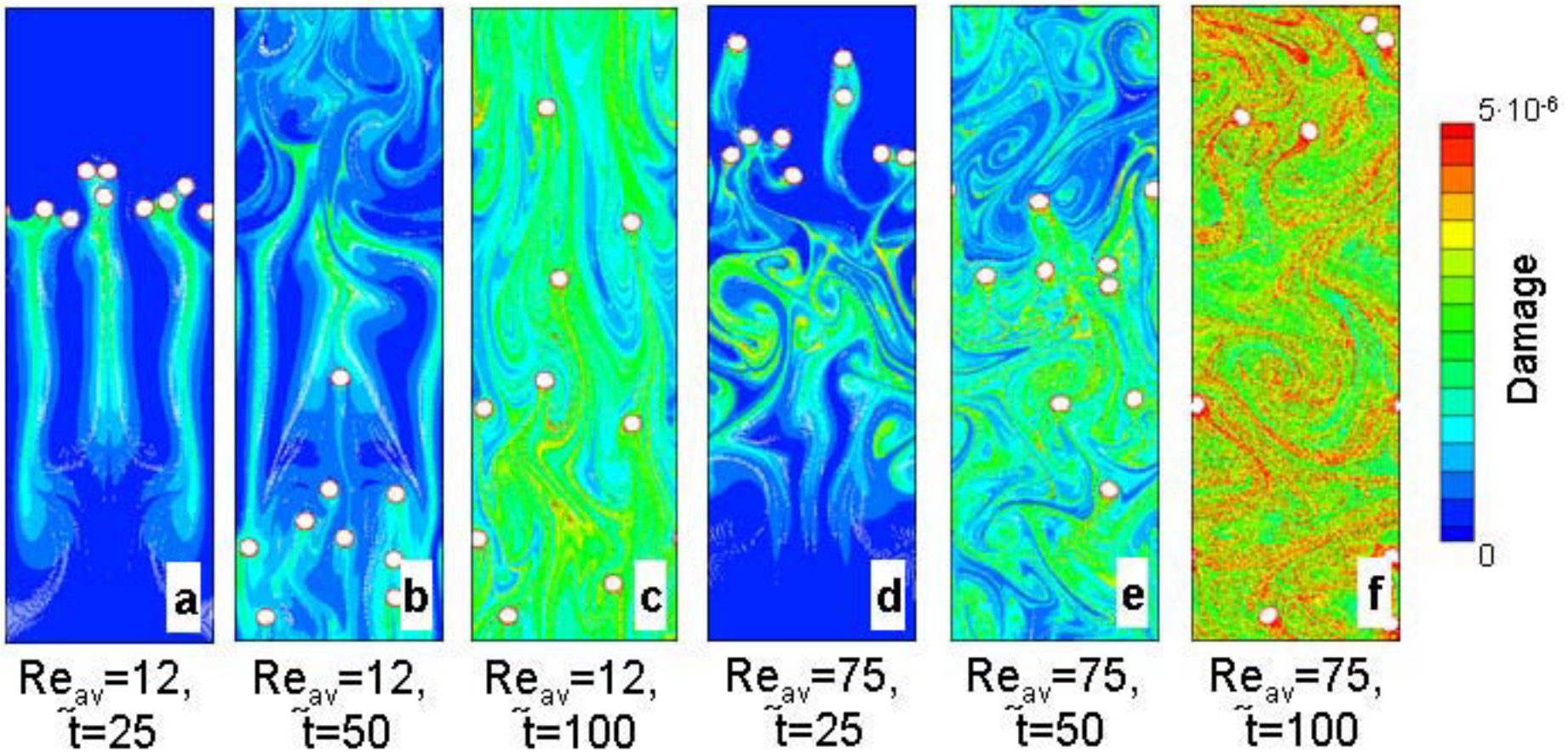

Figure 7. Shear-induced stress level cells around nine bubbles rising simultaneously (Red – high damage, blue – low damage) at different times for a) Re_{av}=12, $\tilde{t}$=25; b) Re_{av}=12, $\tilde{t}$=50; c) Re_{av}=12, $\tilde{t}$=100; d) Re_{av}=75, $\tilde{t}$=25; e) Re_{av}=75, $\tilde{t}$=50 and f) Re_{av}=75, $\tilde{t}$=100.

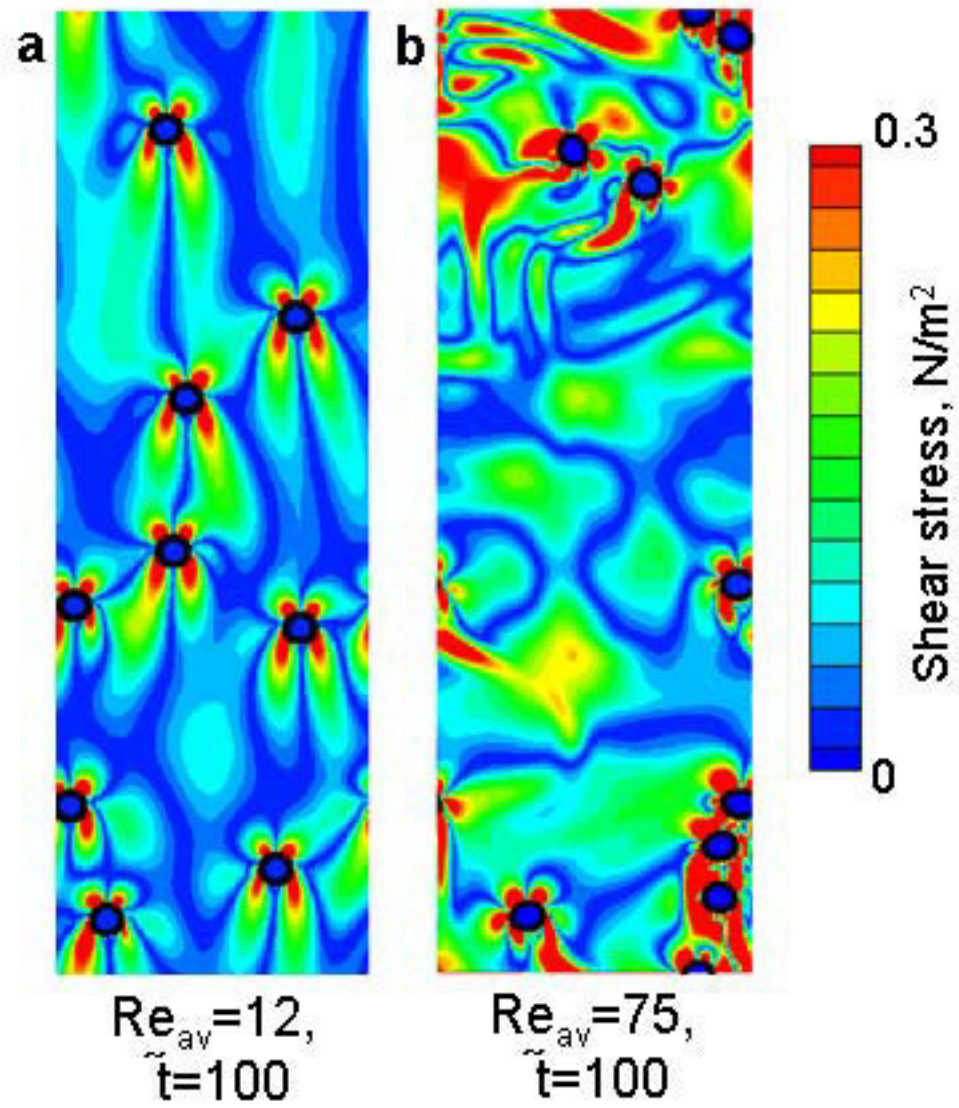

Figure 8. Shear stress fields around multiple rising bubbles (blue –low, red-high) for a) Re_{av}=12, $\tilde{t}$=100 and b) Re_{av}=75, $\tilde{t}$=100.

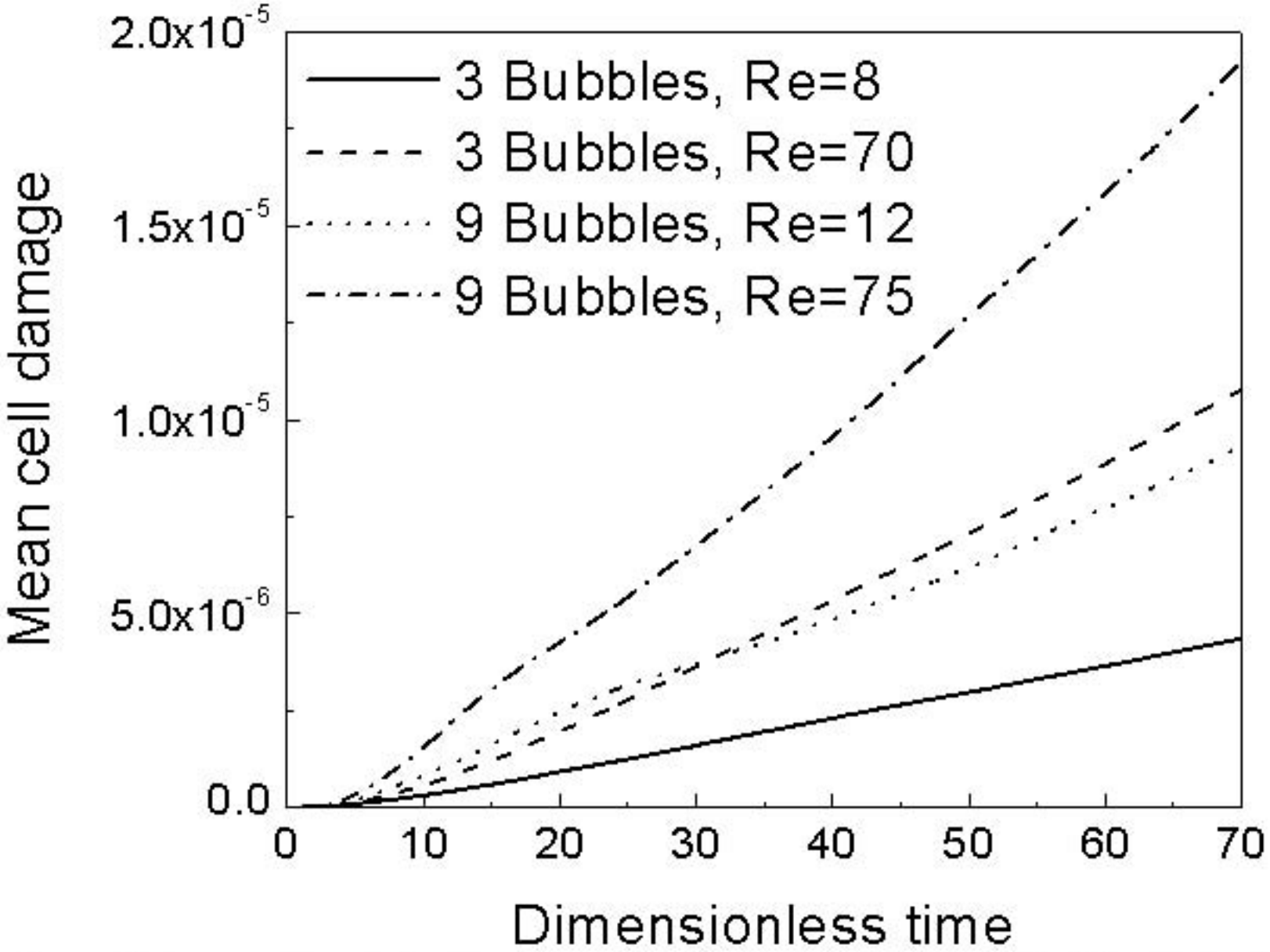

Figure 9. Average shear-induced cell stress level with time for different bubble cluster flow cases.

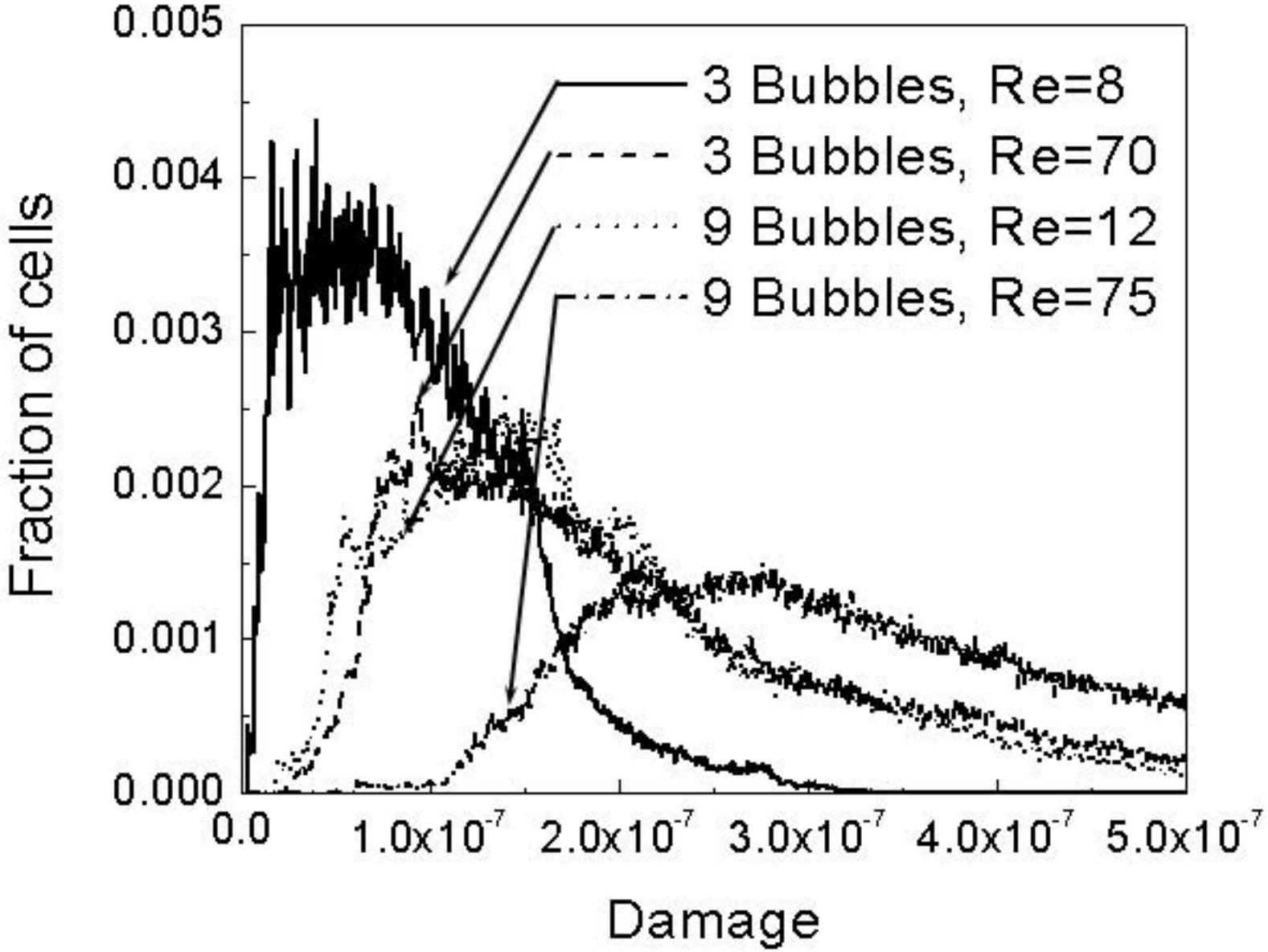

Figure 10. Fraction of cells having been exposed to a certain amount of shear stress in the liquid flow past rising bubble clusters at time ($\tilde{t}$=75).

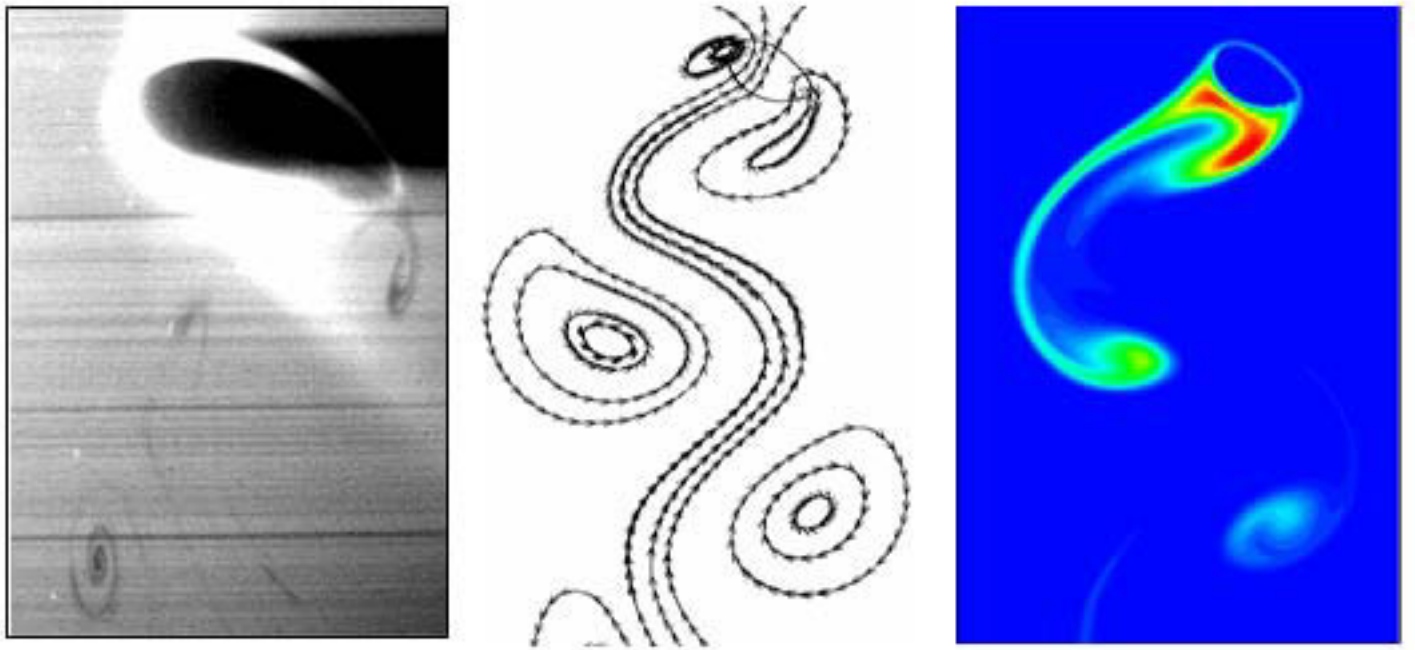

Figure 11. a.) LIF image of the oxygen concentration field around a bubble rising in the vortex-shedding regime in a viscous solution (brightness decrease with increasing oxygen concentration) *Bork et al., (2003)*, b.) Stream-traces associated with the velocity field around a bubble rising in the vortex-shedding regime (Re=68), c.) Numerically obtained dissolved oxygen concentration (Re=68, Sc=60).

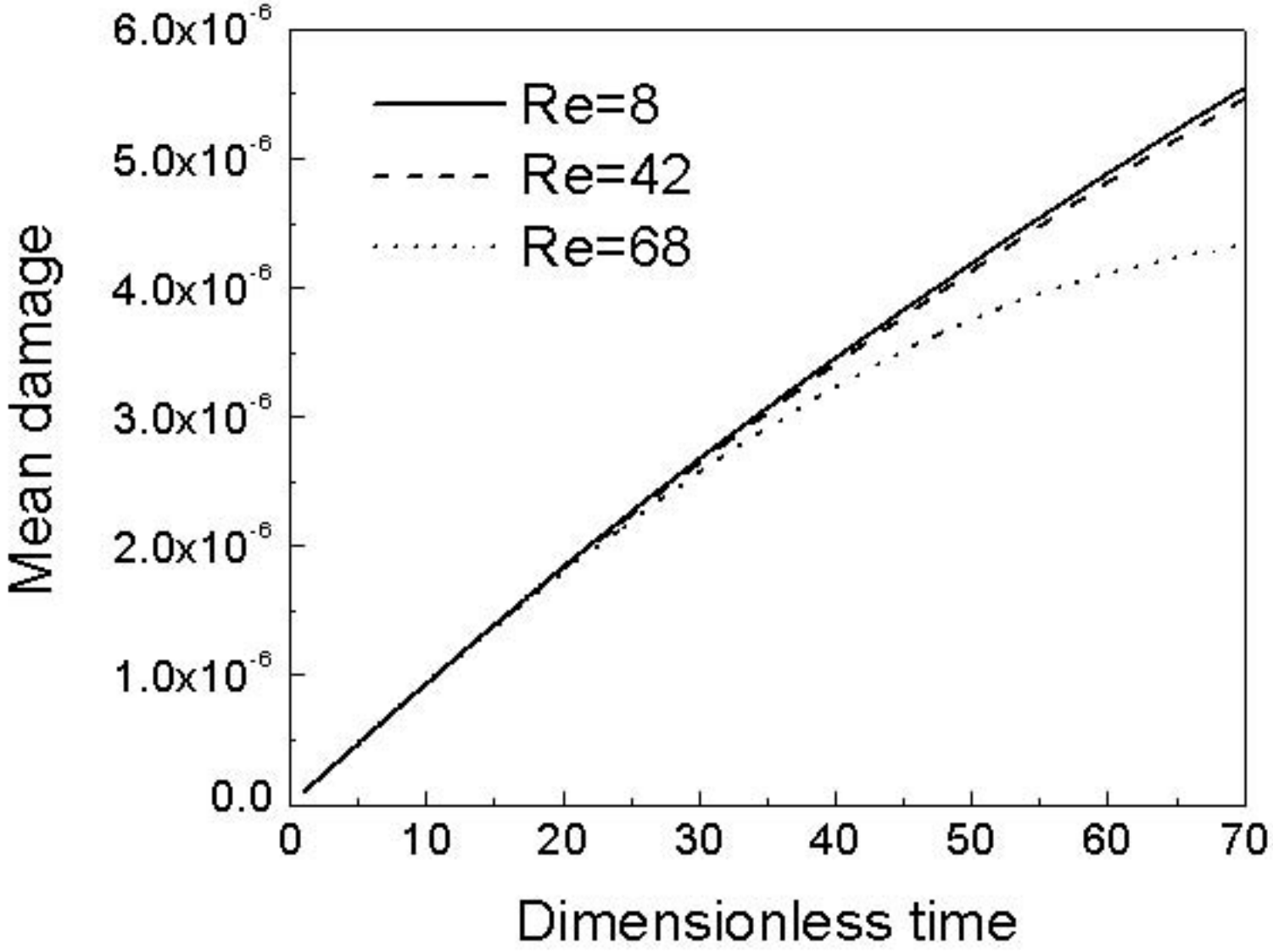

Figure 12. Average hypoxia-induced cell damage with time for different individual bubble flow cases.

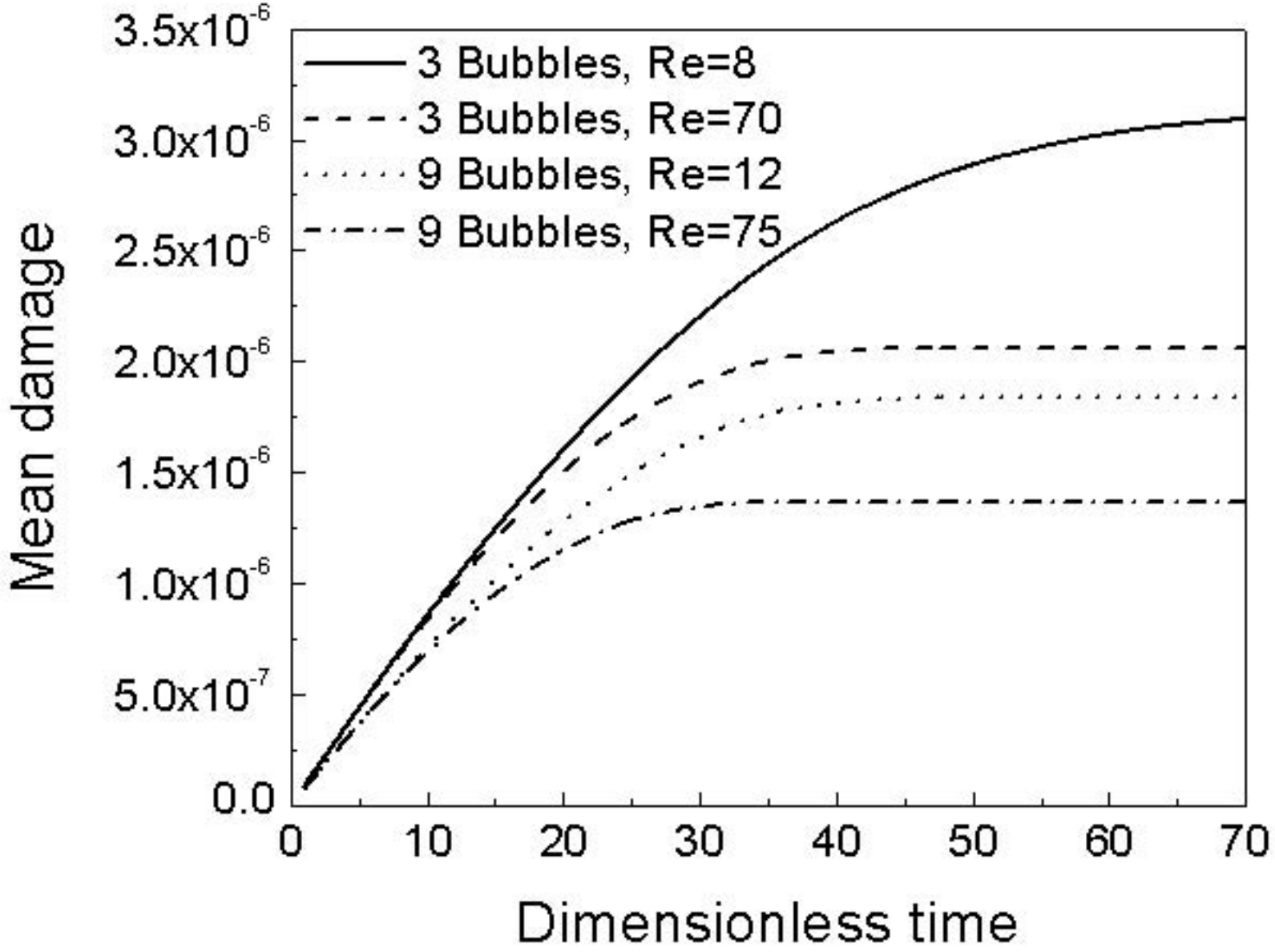

Figure 13. Average hypoxia-induced cell damage with time for different bubble cluster flow cases.

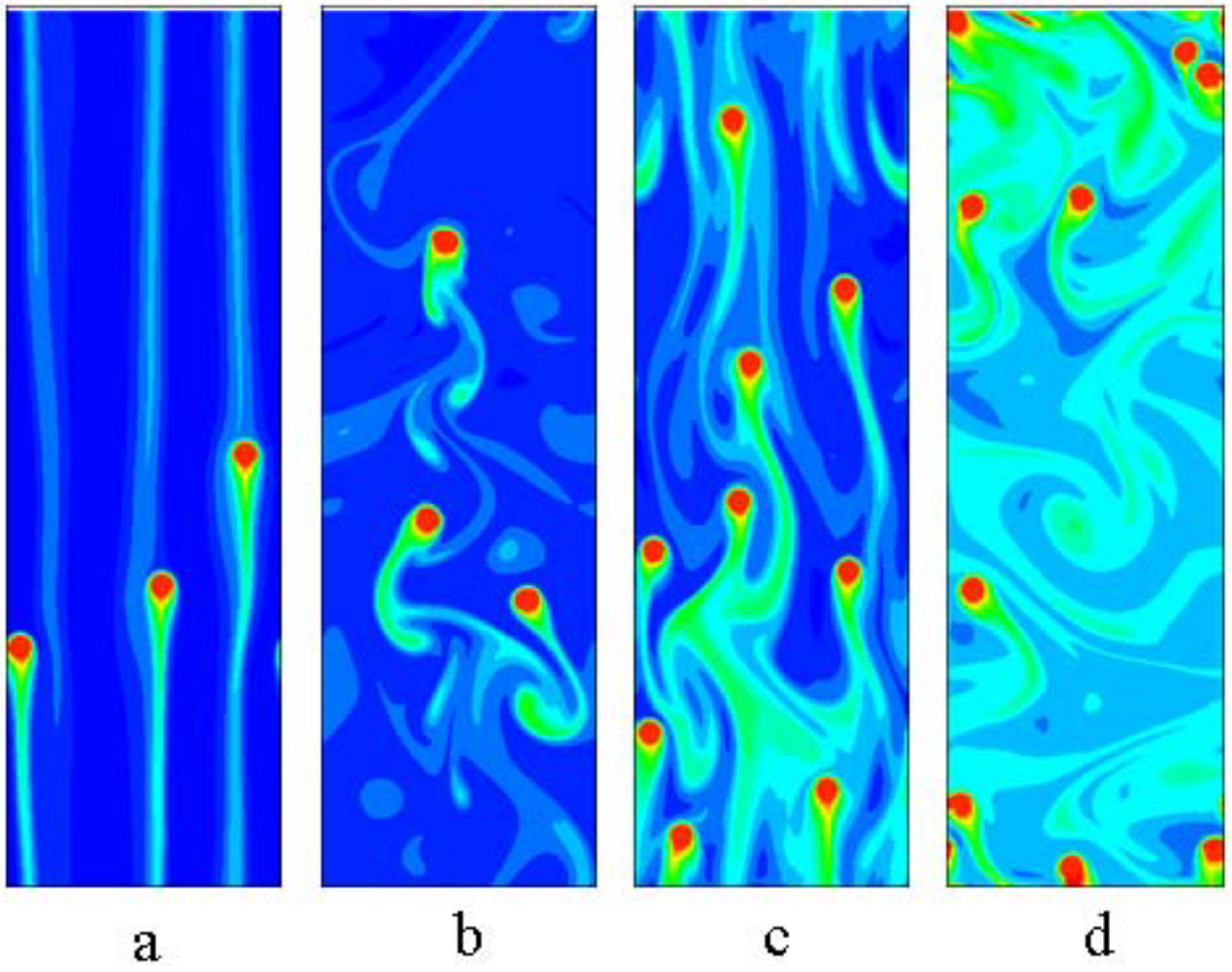

Figure 14. Numerically obtained dissolved oxygen concentration a.) Re=8, Sc=420, 3 bubbles; b.) Re=70, Sc=60, 3 bubbles ; c.) Re=12, Sc=280, 9 bubbles; d.) Re=75, Sc=56, 9 bubbles.